



1 **Paleoseismological evidence of multiple, large**
2 **magnitude earthquake surface ruptures on the active**
3 **Mt. Morrone normal fault, central Apennines, Italy**

4 **Irene Puliti^{*1}, Alberto Pizzi¹, Stefano Gori², Emanuela Falcucci², Fabrizio**
5 **Galadini², Marco Moro², Michele Saroli³**

6 ¹ Dipartimento InGeo - Università G. d'Annunzio di Chieti-Pescara, Chieti (Italy)

7 ² Istituto Nazionale di Geofisica e Vulcanologia - INGV, Roma (Italy).

8 ³ DICeM-Università degli Studi di Cassino e del Lazio meridionale, Cassino (Italy).

9 Corresponding author e-mail: irene.puliti@unich.it

10 **ABSTRACT**

11 The Mt. Morrone active normal Fault (MMF) and the related Sulmona intermountain basin constitute one of the most
12 characteristic examples of the extensional tectonic landscape carving the central Apennines (Italy). Above the ~22 km
13 MMF, thousands of inhabitants concentrate on a thriving reality and a historical and cultural heritage of great significance.
14 According to the current knowledge, the last activation event of the whole MMF occurred ~2000 years ago and the
15 maximum expected magnitude is M 6.6-7. Thus, the MMF today constitutes one of the most problematic structures in the
16 central Apennines seismotectonic setting in terms of large-magnitude earthquake probability. Despite this, information on
17 the activity of the MMF is presently relatively few, both for associated historical seismicity and paleoseismological data. To
18 strengthen these knowledge weaknesses, we performed new extensive paleoseismological analyses (employing four
19 trenches) in the central sector of the fault. Our goal was to supplement the limited existing dataset, constituted by a single
20 paleoseismological study close to the northwestern tip of the fault. Additionally, we aimed to incorporate findings from a
21 pair of studies focused on archaeoseismological and speleoseismological secondary evidence. Through these analyses,
22 we unveiled four significant surface rupture events of the MMF, three of which occurred over the past 6000 years BP.
23 Specifically, the youngest identified event occurred after 3.6-3.5 kyr BP, being thus chronologically consistent with the
24 event in 2nd century CE; a penultimate event after 4.4 kyrs BP; a previous event occurred after 5.4-5.3 kyr BP; and the
25 oldest event took place after 9-8.9 kyr and (presumably) before 5.8-5.7 kyr BP. Considering that the cumulative minimum
26 vertical displacement estimated encompassing the last three events is ~140 cm, and based on the length of the fault at
27 the surface, we can confirm that earthquakes with M 6.6-7.0 may be expected from the activation of the MMF with an
28 inferred average recurrence interval not longer than 1800 years over the last ~5.4 kyr.

29 **KEYWORDS:** Earthquake Geology, Active faults, Surface Faulting Hazard, Paleoseismology, Central Apennines.

30 **1 Introduction**

31 The main parameters useful for fault-based seismotectonic analyses of seismically active regions are the magnitude, the
32 recurrence interval of past earthquakes on a fault, the last event of fault activation and the fault geometry (McCalpin, 2009).
33 Studying the Holocene seismic history of a fault constitutes a necessary task to improve our knowledge of how the fault
34 has ruptured in the past and how it might behave in the future. Therefore, answering the question of the Holocene rupture
35 history (from which the repeat of maximum credible earthquakes is to be derived) for each fault of a given system is a
36 relevant goal to achieve.



37 However, linking the magnitudes of historical earthquakes to a particular active fault is often challenging and depends on
38 the quality of historical catalogues and the conservation of the geological traces of fault ruptures in the landscape. In this
39 regard, the Sulmona basin is bounded by one of the major active normal faults of the central Apennines, the so-called Mt.
40 Morrone Fault (hereafter MMF) and it was hit by several historical earthquakes of $M_w > 5.7$ and up to about $M_w 7$,
41 generated by adjacent seismogenic sources (Rovida et al., 2022). Nonetheless, none of them is presently associated with
42 the MMF activity, albeit the origin of some of them is still debated. Such uncertainty stimulated researchers to investigate
43 the seismic history of the MMF and its seismogenic behaviour, either at long- or short-term scales.

44 In the absence of recent occurrences of seismic events, paleoseismological trenching has been worldwide proven to be
45 the most efficient approach for past fault rupture detection in active tectonic contexts (e.g., Manighetti et al., 2007; Duross
46 et al., 2016). On the other hand, trenching provides punctual information that might not be representative of the entire fault
47 system deformation, because both coseismic and long-term slip distribution can vary significantly along the length of a
48 fault, especially across complexities (e.g., Iezzi et al., 2018; 2023; Puliti et al., 2020). Indeed, different potential scenarios
49 of the distribution of surface ruptures can occur during earthquakes along the causative fault, due to several possibly
50 interacting factors not easily discernable a priori.

51 At present, a sole paleoseismological investigation has been conducted on the MMF by Galli et al. (2015), from which four
52 paleoearthquakes over the last ~ 9 kyr have been retrieved. However, this represents an isolated spot located in the
53 northern portion of the fault, and therefore it might not provide a compelling picture of how the fault ruptured and what the
54 maximum expected event is (in terms of fault surface offset).

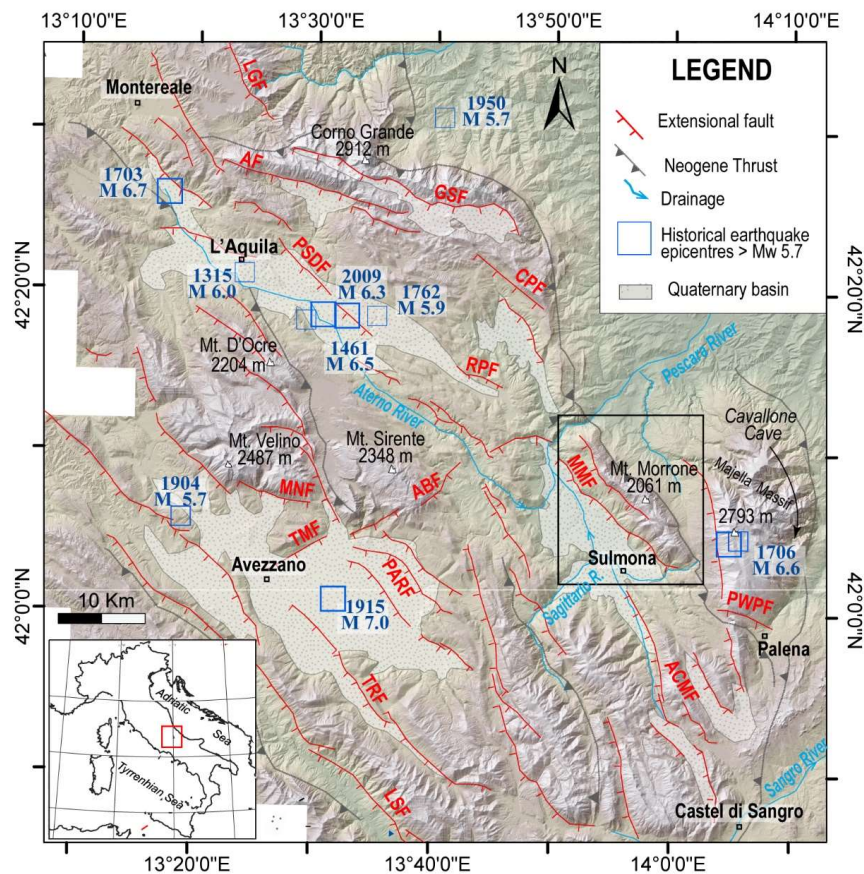
55 In this regard, the present study focuses on enlarging the paleoseismic records of the MMF and extending back the seismic
56 history retrieved on different portions of the same fault, to provide a reliable rupturing scenario at fault system-scale. We
57 conducted a paleoseismological investigation at the central portion of the MMF, close to Roccasale village, which
58 according to the classical fault evolution model, is expected to record the highest vertical displacement (e.g., Walsh and
59 Watterson, 1987; Peacock and Sanderson, 1991), thus providing with more significant pieces of evidence regarding the
60 actual surface displacement potential (that can be related to the maximum earthquake size generated by the fault; e.g.,
61 Wells and Coppersmith, 1994). We here describe the results of the new paleoseismological analysis performed along the
62 MMF through four trenches dug in a sector of the fault trace well expressed in the local morphology. As shown in the
63 discussion, the analysis of the obtained results allows us to attempt to define the fault rupture's dimensions and geometry,
64 and the timing of seismic events, which should be more representative of the maximum behaviour of the fault. Finally, we
65 discuss these results and observations in comparison with the existing paleoseismological study (i.e., Galli et al., 2015) to
66 unravel the short-term fault deformation at a system scale.

67 2 Regional tectonic setting

68 The Apennine chain results from the complex interaction between the African and European plates and the Adria microplate
69 since the Late Oligocene-Miocene. The westward subduction of the Adriatic lithosphere beneath Europe and its
70 progressive eastward flexural retreat produced an NE verging foreland thrusts-and-folds system involving Mesozoic-
71 Cenozoic carbonate rocks in the central Apennines with a contemporaneous back-arc opening of the Tyrrhenian Sea
72 (Boccaletti et al., 1990; Cipollari et al., 1999; Cipollari and Cosentino, 1995; Doglioni, 1991; Patacca et al., 1990). The
73 contractional structure is characterised by NW-SE striking anticlines bordered at their forelimbs by gently southwest-
74 dipping thrust fronts (Ghisetti and Vezzani, 1997). Since the Late Pliocene-Early Pleistocene, SW-NE extensional tectonics
75 overprinted the contractional deformation, with active normal faults generally trending parallel to the chain axis and dipping
76 to the SW, affecting the axial zone of the chain, and becoming progressively more recent toward the Adriatic Foreland (i.e.,
77 to the East) (e.g., Lavecchia et al., 1994; Piccardi et al., 1999; Galadini and Messina, 2004). Alongside newly formed
78 normal faults, the extensional deformation also re-used fault planes inherited from the compressive phase (Calamita and
79 Pizzi, 1992; Cavinato and Cosentino, 1994; Falcucci et al., 2018; Pucci et al., 2019).



80 In the central Apennines, the activity of normal fault systems has led to the formation of several graben or half-graben
81 structures corresponding to intermountain basins (e.g., Fucino, Sulmona, L'Aquila, and Norcia basins) located in the
82 hanging walls of the main normal faults. These basins hosted continental depositions filled with Plio-Quaternary
83 successions (e.g., Bosi and Bertini, 1970; Bosi et al., 2003; Pucci et al., 2015; Puliti et al., 2022) (Fig. 1). The normal fault
84 activity over Quaternary is testified by evidence of displaced continental deposits and landforms. The present extensional
85 activity is also testified by the historical seismicity (earthquakes with magnitudes of up to 7.0 in the past millennium, e.g.,
86 Rovida et al., 2022), instrumental seismological data (e.g., Chiaraluce et al., 2017; Pondrelli et al., 2010; Ekstroem et al.
87 1998), that indicate earthquake ruptures compatible with extensional faulting, and by several studies dealing with active
88 tectonics and paleoseismology (e.g., Galadini and Galli 2000; Galli et al., 2008).



89
90 **Figure 1.** Structural framework of the Abruzzi region and historical seismicity of the Abruzzo region fault systems modified after
91 Puliti et al., (2024); acronyms define faults considered as active: Laga-Gorzano Fault system (LGF), Gran Sasso Fault system (GSF),
92 Assergi Fault (AF), Mt. Cappucciata Faults (CPF), Paganica San Demetrio Fault System (PSDF), Roccapreturo Fault (RPF), Magnola-
93 Velino Faults (MNF), Tre Monti Fault (TMF), Parasano Fault (PARF), Trasacco Fault (TRF), Liri Southern Fault (LSF), Mt. Morrone Fault
94 (MMF), Aremogna- Cinque Miglia Fault System (ACMF). The Palena–western Porrara fault (PWPF) is from Pizzi et al. (2010). The
95 Avezzano-Bussi Fault (ABF) is from Gori et al., (2017). The shaded relief derives from 20 m DEM. Historical earthquake epicentres
96 (>Mw 5.7) are from catalogue CPTI15 (Rovida et al., 2022). Major Neogene thrusts are indicated in grey (Ghissetti and Vezzani, 1997).
97 The blue fault indicates an ENE-WSW striking. The investigated area is outlined by the black rectangle.



98

99

2.1 Geological setting of the Mt. Morrone Fault (MMF)

100

The Mt. Morrone ridge is in the outer portion of the Central Apennine range. It represents an anticline structure related to northeast-verging thrust that was active during the Late Messinian to the Early Pliocene (e.g., Cipollari and Pipponzi, 2003).

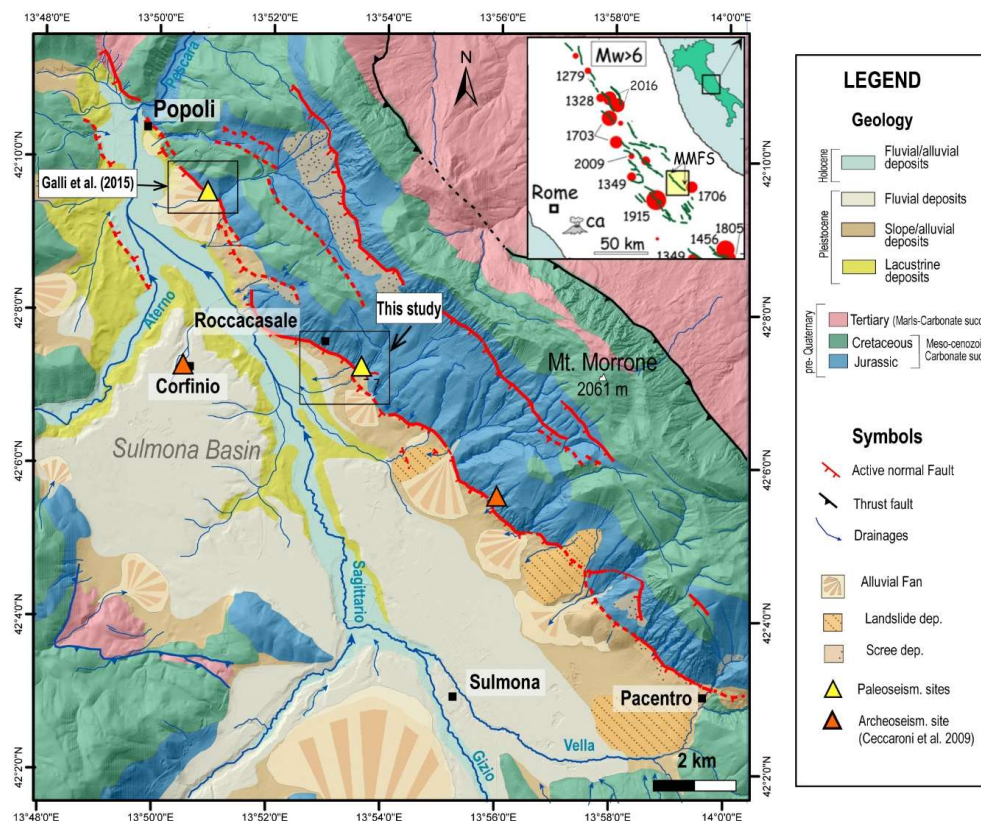
101

The thrust fault, outcropping along the eastern limb of Mt. Morrone, superimposed Meso-Cenozoic limestones, over

102

103

Cenozoic (Neogene) terrigenous deposits (Fig. 2).



104

Figure 2. Simplified geological map of the Mt. Morrone Fault (MMF), modified from CARG geological sheet “369 Sulmona” (Servizio Geologico d’Italia, 2006). Locations of the paleoseismological study of Galli et al. (2015) and this study are reported, and yellow triangles indicate the excavation sites. The orange triangles are some of the archaeological sites reported in the archaeoseismological study by Ceccaroni et al. (2009). In the inset: the locations of primary active faults in Central Italy and $6 < M < 7$ earthquakes are shown, modified from Galli et al. (2015). The yellow rectangle marks the area in which the MMF is located.

105

106

107

108

109

110

111

The back limb of the Mt. Morrone anticline was then affected by a ~22 km-long, NW-SE striking normal fault giving rise to the Sulmona Basin, a ~7 km wide half-graben intermontane depression that bounds the Mt. Morrone ridge all along its length. The Sulmona Basin is filled with Quaternary sedimentary succession, which has been described in several studies (e.g., Demangeot, 1965; Vittori and Cavinato, 1995). According to them, the depression hosted a fine-grained lacustrine deposition > 400-500 m thick since the Early Pleistocene (Cavinato and Miccadei, 2000; Giaccio et al., 2009; Miccadei et al., 1998). Afterwards, the continental sedimentation was dominated by an Upper Pleistocene coarse-grained alluvial sedimentation mainly driven by the Vella, Gizio, Sagittario, and Aterno Rivers and by the drainages from the Mt. Morrone western flank. The southern area of the Sulmona basin has also been affected by landslide deposits derived from large-

112

113

114

115

116

117

118



119 scale gravitational movements that occurred from the Early to Late Pleistocene, according to the available literature (e.g.,
120 Miccadei et al., 1998; Gori et al., 2014).
121 The extensional active MMF comprises two main parallel fault branches from Popoli to Pacentro: the western and eastern
122 fault branches (e.g., Gori et al. 2010 and references therein), whose related scarp are found at different elevations along
123 the slope (400-800 m a.s.l. and 1200-1500 m a.s.l. respectively). The highest and easternmost branch, defined as the
124 "Schiena d'Asino Fault" (Ciccacci et al., 1999; SAF, after this), is located at Mt. Morrone peak's foot, and it is made of an
125 at least 14 km-long main bedrock fault scarp on the central-northern portion of the mountain range at the base of which
126 the fault plane is nearly continuously exposed.
127 The western fault branch is at a lower elevation, and it bounds the Sulmona basin all along its extent. It strikes N140° from
128 the northern tip up to the central portion (north of Roccacasale village) and N155° southward. Locally, some splays, like
129 the fault portions at Roccacasale, strike from N155° to E-W oriented. The fault plane is visible at the base of the fault scarp
130 along several sections from Popoli to the north, to Pacentro, to the south, of about 3-5 km long each. The kinematic
131 indicators measured along the fault planes show a prevalent normal dip-slip movement, however on the NNW-SSE and
132 near E-W striking planes a slight left and right oblique component is observed, respectively, in agreement with a main NE
133 extension direction (e.g., Pizzi and Pugliese, 2004). For the basin-bounding fault, a minimum age of 268 kyr BP has been
134 estimated from U-Th dating of carbonate mineralizations linked to the coseismic rejuvenation, with a 10–15-kyr cyclicity,
135 of the structural permeability in the fault zone (Vignaroli et al., 2022). By measuring the displacement of the Quaternary
136 deposits (aged since the Early Pleistocene) outcropping on both sides of the Sulmona basin, a minimum offset of 350 m
137 is estimated to be accommodated by the western fault branch (Gori et al., 2007; 2014; Miccadei et al., 2004), based on
138 the displacement of the Early Pleistocene Mt. Orsa Breccias outcropping at Mt.Orsa and close to the Sagittario Gorge. As
139 for the late Quaternary kinematic history, **Late Pleistocene-Holocene deposits are displaced** along the western fault splay
140 of up to about 20 metres, attesting to a slip rate of the branch on the order of **0.4 mm/yr** (Gori et al., 2010; Puliti et al.,
141 2024).

142 *2.1.1 Historical seismicity and previous paleoseismological investigations of the MMF*

143 The Sulmona area was hit by several historical earthquakes of $M_w > 5.7$ and of up to $M_w 7$, namely the 1349, 1456, 1706,
144 1915, and 1933 events (Rovida et al., 2022). However, none of them were associated with the MMF activity, but with
145 adjacent seismogenic sources, albeit the origin of some of them is still debated. An example is the 1706 Majella earthquake
146 tentatively associated with a thrust or backthrust fault reactivation by some authors (De Nardis et al., 2008; Galli et al.,
147 2019), even if no conclusive data supporting this hypothesis has been found to date. This open issue stimulated
148 researchers to investigate the seismic history of the MMF.
149 **Aerchaeoseismological** investigations in the Sulmona basin area cast light on the occurrence of a strong local earthquake
150 in the half of the 2nd century CE (Galadini and Galli, 2001; Ceccaroni et al., 2009). From the reconstructed shaking scenario,
151 a consistency between the event and the activation of MMF has been found. The written source related to this earthquake
152 is represented by an epigraph mentioning the restoration of a damaged weighing house at an ancient locality about 18 km
153 north of Sulmona. In the available seismic catalogues, it is reported with the conventional date of 101 CE, an epicentral
154 intensity I₀ 9–10 of the MCS scale, and an estimated magnitude $M_w 6.3$. Faulting evidence and radiocarbon dating from
155 paleoseismological trench studies close to Popoli (see location in Fig. 2) performed by Galli et al. (2015) corroborated the
156 occurrence of MMF activation in a period consistent with the second-century AD seismic event, besides three prior faulting
157 events, occurred in the past ~9 ky BP, with the most recent constrained, indeed, as the middle of the 2nd century CE.
158 On a regional scale, the MMF has also been associated with seismic events recorded on speleothems in the Majella Massif
159 (Cavallone Cave). In the cave, large collapses of cave ceilings, fractures, broken speleothems, and radiocarbon dating of
160 new re-growing stalagmites on their top, together with other coeval off-fault geological data collected in surrounding areas
161 outside the cave (i.e., wooden samples in the Palena rock avalanche), provide important constraints for the individuation
162 of a mid-Holocene paleo-earthquake occurred around 4.8 – 4.6 kyr BP and post 5.4-5.3 kyr BP, respectively (Di Domenica

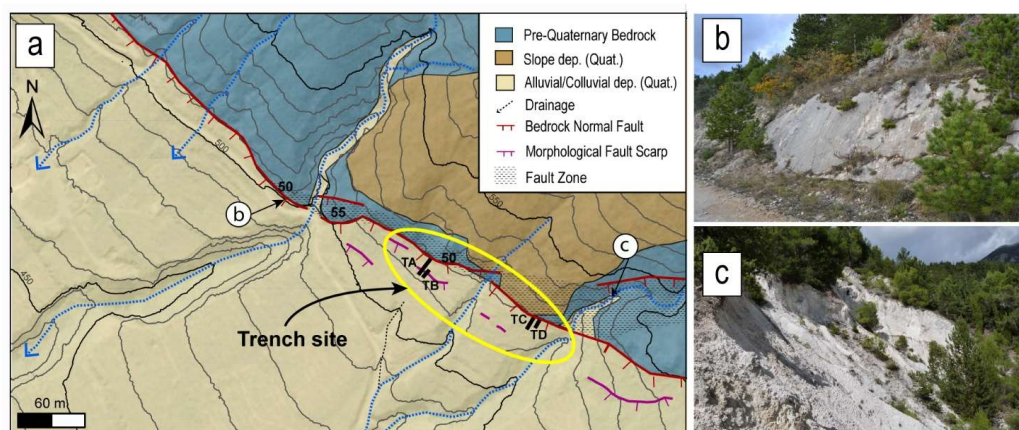


163 and Pizzi, 2017). The authors also postulated the observed effects on speleothems were caused by an earthquake with a
 164 magnitude larger than that supposed by the activation of the sole MMF, hypothesizing the conterminous rupture of other
 165 nearby active faults, causing earthquakes of magnitude around 7. In this perspective, assuming that the MMF is a
 166 “segment” of a larger seismogenic source comprising also the Palena and Mt. Porrara active normal faults (Fig. 1) of Pizzi et
 167 al. (2010) and Gori (2010) located just SE of the MMF and aligned with it, Bordoni et al. (2023) calculated that they are capable of
 168 rupturing together with Mw about 7 earthquakes.

169 3 Paleoseismology of the Monte Morrone Fault System

170 3.1 Study area

171 Based on the geological and geomorphological background and the new observations and data acquired in the field, we
 172 investigated the central portion of the MMF, close to the Roccasale village. Here, the western fault splay of the MMF
 173 placed the Mesozoic carbonate limestones, in the footwall, into contact with Quaternary alluvial deposits, in the hanging
 174 wall (Fig. 3a). The fault is expressed as a 2 km-long bedrock fault scarp at the base of which the fault is exposed, with an
 175 N110° strike and dipping 50°-55° SSW toward the Sulmona basin (Fig. 3b). The fault zone in the footwall consists of
 176 Jurassic carbonate bedrock characterized by a several tens of metres of where multiple secondary parallel fault splays
 177 accommodate the brittle deformation (Fig. 3c).



178

179 **Figure 3.** a) Simplified geological map of the study area. The four trenches are indicated by the black segments within the
 180 yellow ellipse. The contour lines are 10 metres each, and the field picture's location is indicated. B) Field picture of the
 181 Roccasale fault slip plane outcropping along the road. C) Field picture of the Roccasale cataclastic fault zone.

182 The hanging wall block consists of confluent alluvial fans from the slope of Mt. Morrone, leading to a well-stratified alluvial
 183 depositional sequence that dips gently towards the Sulmona basin, in literature is indicated as deposits from the Upper
 184 Sulmona Terrace (UST; Miccadei et al., 1998), which has its wider outcrop in a 30 m-thick succession, exposed by drainage
 185 incisions. The age of the alluvial deposits is constrained up to 36-40 kyr according to a tephra layer embedded in the
 186 deposits, five metres below the topographic surface (Gori et al., 2011; Galli et al., 2015), and the exposure dating of the
 187 surface by cosmogenic nuclides concentration (Puliti et al., 2024). Colluvial sediments locally covered the alluvial bodies.
 188 Stream incisions cutting through the alluvial sedimentary bodies show the presence of several synthetic and antithetic fault
 189 strands affecting these deposits, close to the main fault zone. They reflected in the morphology of the hanging wall, where



190 field observations and morphostructural study highlighted the presence of further fault scarps of a ~10-20 m length, parallel
191 to the main carbonate one. Unfortunately, most of these scarps have been severely altered by widespread agricultural
192 practices over centuries. Indeed, human activity has obscured or re-elaborated much of the cumulative fault scarps, leaving
193 only a few sites where relatively undisturbed Late Pleistocene/Holocene morphotectonic features are preserved.
194 We selected the paleoseismological study site 1 km south of the Roccacasale village. Four trenches, named TA, TB, TC
195 and TD, have been excavated with an N 35° orientation, that is perpendicular to the fault scarps (Figg. 3 and 4). The 20
196 m-long TA trench was opened from the bedrock fault plane and across a minor fault scarp, located 15 metres far from the
197 main one. A shorter 6 m-long trench, TB, was dug 4 metres southward, far from trench TA. Two further 5m-long trenches,
198 TC and TD, **some** 5 metres apart from one another, were excavated a hundred metres SE of TA and TB; their location was
199 chosen at the base of the fault plane involving slope breccia and alluvial fan deposits at the footwall. The walls of the four
200 excavations were cleaned and gridded at 1 × 1 m spacing (locally 0.5 × 0.5 m) and prepared for stratigraphic logging and
201 geochronological sampling.



202
203 **Figure 4.** Field pictures of trench TA (left) and trench TB (right).

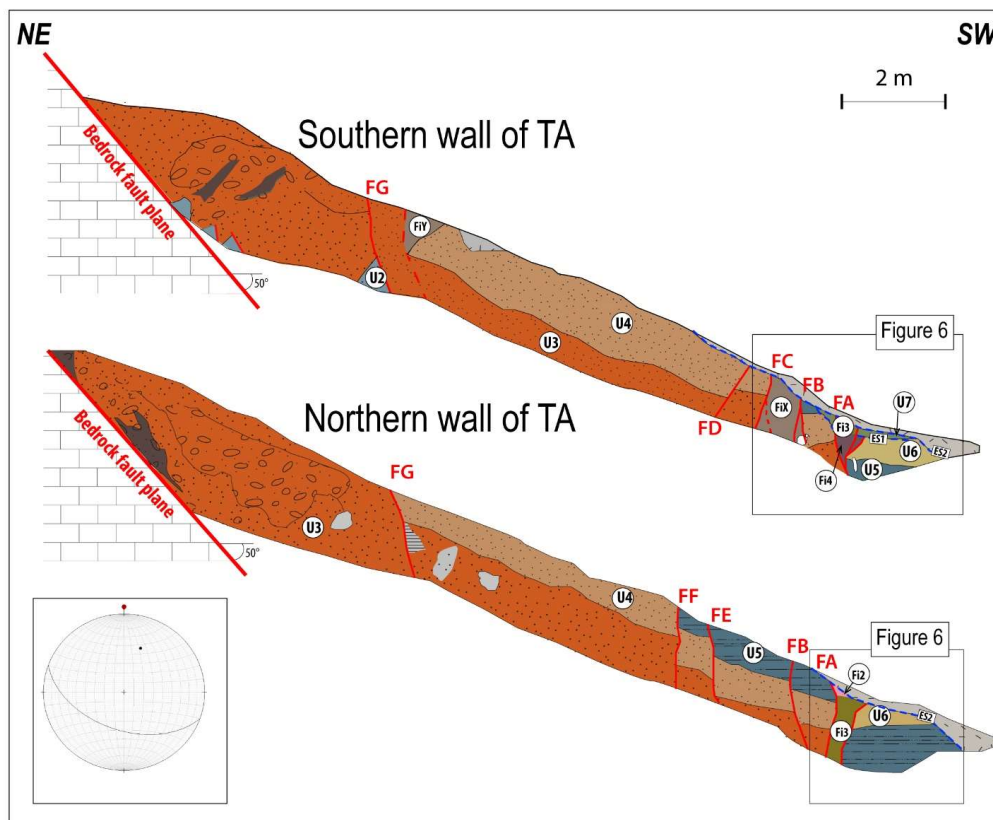
204 We performed radiocarbon dating of organic material and charcoal shards incorporated in the sediments, to obtain
205 chronological constraints for the stratigraphic sequences exposed by the trenches. Further, to compare the results and
206 ensure reliable ages, our radiocarbon samples (charcoals and bulk) have been sent to **two different specialised laboratories**
207 (Beta Analytics Laboratory, Florida, USA, and CEDAD-Centro Datazione e Diagnostica of Salento University- Italy). The
208 measurements were performed through AMS analysis and calibrated through BetaCal3.21 and OxCal3.10 in the two
209 laboratories. The radiocarbon ages used in this work have been corrected according to Ramsey (2009) and Reimer et al.
210 (2013) and then reported as BP.



211 3.2. The TA and TB Trenches

212 **3.2.1. Stratigraphic setting of Ta and TB**

213 The deposits of the TA and TB trenches have been analysed. Some of the units exposed by the two trenches were
214 comparable by sedimentary characteristics which, considering also the proximity of the two sites, suggests a shared
215 stratigraphy. We distinguished 8 stratigraphic units whose order follows their chronostratigraphic position numbered from
216 1-the oldest in both excavations, up to 8-the youngest (Fig. 5 and 6). We also identified and labelled sediments infilling
217 paleo-fissures as Fi, from the older Fi4 to the younger Fi2 that, as exposed below, we associated with subsequent events
218 of fault activations. With FiX and FiY we named additional infilling sediment that could be older than Fi4, but the lack of the
219 complete geological record prevents any chronological constraint of these infilling units.



220
221 **Figure 5.** Stratigraphic sketch logs of the Trench TA's southern and northern walls. The northern wall log is mirrored (to
222 its actual appearance) to highlight the correspondence between the two walls. The stereo plot indicates the bedrock fault
223 plane measured at the top end of the trench (200/50). Units and faults, marked by red lines, are labelled in the figure.

224 The oldest depositional body of the stratigraphic sequence is unit U1, outcropping in the trench TB. It is made of
225 interfingered slope and alluvial fan deposits and comprises whitish, and carbonate stratified breccias containing orange,
226 sandy levels 20 cm thick dipping 15°.



227 Unit U2 is made of light-yellow calcareous sand at the base with a coarsening upward trend, matrix-supported with very
 228 small clasts up to 2-3 mm in the upper part. This unit outcrops in small patches at the base of the southern wall of the
 229 trench TA.

230 Upward, the stratigraphic sequence continues with unit U3, found extensively along the entire TA trench walls: a medium-
 231 to-fine calcareous of red to orange sandy deposit, with sparse and small clasts (5 mm) and an average thickness of 60-70
 232 cm up to 2 m close to the bedrock fault plane. U3 shows continuity along the TA trench walls, with a coarsening upward
 233 texture and an upward increase of consolidation. The massive aspect and thickness of sandy deposits were recognized to
 234 be associated with sediment-laden processes, producing hyper-concentrated sandy slope deposits (Benvenuti and Martini,
 235 2009). Commonly, in continental systems, these sands are matured and temporarily stored in coeval continental
 236 depositional environments, where they are periodically removed and transferred into the basin by rivers during major floods
 237 (Zavala, 2020).

238 The subsequent unit U4 shows a thickness of 40-75 cm, composed of very coarse calcareous sand that is nuanced from
 239 orange to hazelnut. It is a dense deposit with small clasts from 2 to 10 mm organized in small patches and abundant
 240 reworked tephra minerals. A 10 cm-thick coarse layer, thinning eastward, marks the contact with the unit below.

241 The southwesternmost portion of the excavation of TA (Fig. 6) and the trench TB exposed the youngest preserved deposits,
 242 all represented by fine-grained colluvial deposits with attitude conformable to the slope. Unit U5 is a silty colluvium with
 243 yellowish-brown/grey sand, having ~100 cm of minimum thickness, with rare carbonate clasts. The base of unit U5 is
 244 characterized by a gravel matrix-supported layer with clasts from 1 to 10 mm (locally sub-rounded) and parallel to the main
 245 deposition direction.

246 Unit U6 is a sandy brown-to-yellowish 55-65 cm-thick massive colluvium with a few clasts less than 1 cm in diameter. U7
 247 is a deposit composed of an unstratified well-consolidated clast-supported part with 20 cm of thickness, and then, in its
 248 westernmost position, it is a more yellowish sandy deposit 20-25 cm thick, less consolidated with small, rounded carbonate
 249 clasts of 1-2 cm diameter. Radiocarbon dating of charcoal sampled in U7 provided an age of 5830-5749 yr BP (sample
 250 RC2). Given the colluvial origin of the sediments, this age defines a lower chronological limit for the deposition. Two
 251 erosional surfaces, named ES1 and ES2, mark two unconformities between U6 and U7 deposition, and between U7 and
 252 the ploughed soil, respectively. The occurrence of the erosional surface ES2, with anthropogenic genesis due to agricultural
 253 activities, prevented the preservation of the uppermost unit U8, of which we have evidence of its presence only in the
 254 infilling sediment Fi3 described below, which is made at expenses also of this eroded unit. Specifically, U8 was mainly
 255 composed of a dark brown paleosol, from which we collected charcoal fragments that gave an age of 4985-4963 yr BP
 256 (sample RC1, [Table 1](#)).

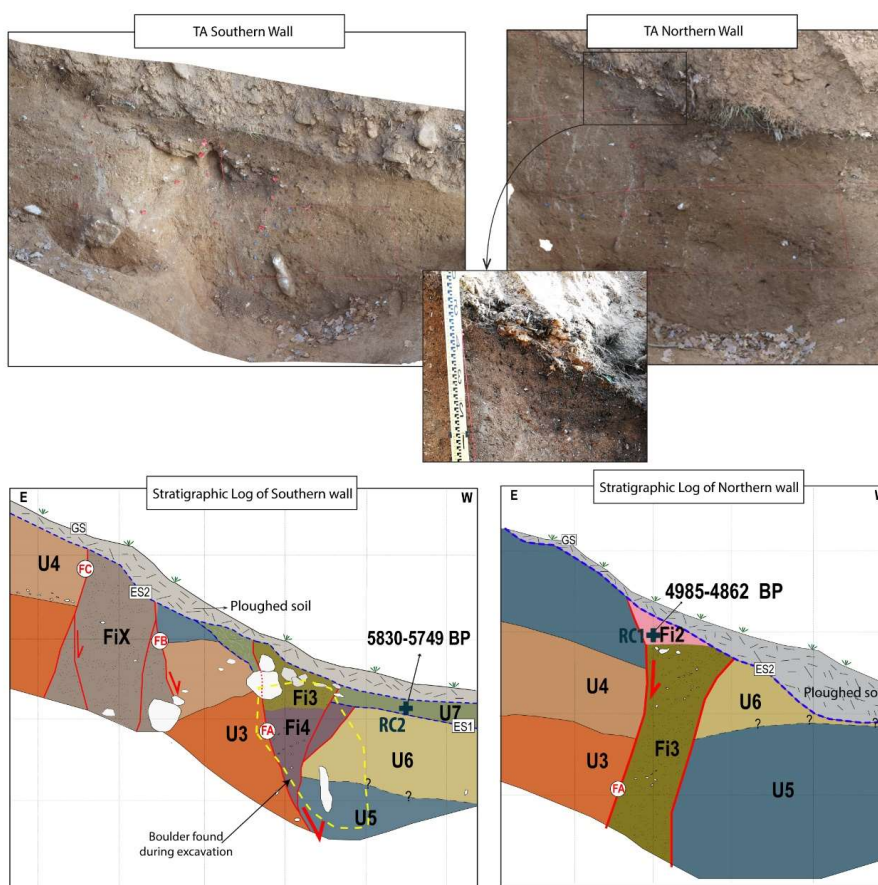
Sample	Trench	Unit	Calibrated Radiocarbon Age	Dated material	Lab
RC1	TA	Fi2	4985-4862 cal yr BP	Bulk	Beta Analytic
RC2	TA	U7	5830-5749 cal yr BP	Detrital Charcoals	Beta Analytic
RC3	TB	Fi3	5424-5320 cal yr BP	Detrital Charcoals	CEDAD
RC4	TB	Fi3	5458-5375 cal yr BP	Detrital Charcoals	Beta Analytic
RC5	TC	U1	3610±30 cal yr BP	Detrital Charcoals	Beta Analytic
RC6	TC	U2	4460±30 cal yr BP	Detrital Charcoals	Beta Analytic

257 [Table 1](#). Radiocarbon dating of samples collected in the investigated trenches. See [Figg. 6-8-9](#) for sample locations.

258 As exposed before, the trench walls showed fissures infilled with sediment from the adjacent units. Specifically, based on
 259 the material contained, four different infilling deposits were identified. The FiY and FiX are both grey-hazelnut silty sands
 260 related to U3-U5, and U3-U4-U5 re-elaboration, respectively; the Fi4 is a dark-grey silty sand with scarce carbonate clast



261 of 1 cm in size with a parent material related to units U5-U6. FiY, FiX and Fi4 can be only observed on the southern wall
 262 of TA.
 263 The Fi3 unit is a dark-brownish silty sand with local yellowish sandy patches. In the northern wall, Fi3 showed several
 264 patches of dark colluvium with carbonate pebbles of 5-10 cm in size. The parent material of Fi3 might be related to units
 265 U5-U6-U7 and to the younger unit U8, which, as described above, should have been a dark brown paleosol removed
 266 during the erosional phase marked by the surface ES2 and preserved only as Fi3 infill. Charcoal samples from Fi3 have
 267 been radiocarbon dated at 5424-5320 yr BP and 5458-5375 yr BP (samples RC3 and RC4, Table 1), indicating that the
 268 infilling deposit occurred after the younger age of the two. The Fi3 deposited above Fi4.
 269 Fi2 has been only observed at the northern wall of TA. It is filled by a silty colluvial deposit unconformably overlaying Fi3.
 270 The radiocarbon age determination of a charcoal shard contained in it gave an age of 4985-4862 BP. From lithological
 271 observations the parent material of Fi2 might be related to U7 and U8. The sequence is truncated at the top by the ES2
 272 erosional surface and sealed by thin-ploughed soil.



273

274 **Figure 6.** Stratigraphic log of the portion of trench TA, southern and northern (mirrored) wall. The inset is a zoomed picture
 275 of the Fi2 colluvial wedge. Unit names and faults are indicated in the figure and referred to in Table 1. ES: erosional
 276 Surface; GS: Ground Surface. The sample's position is indicated with a blue cross. The grid is each 50 cm.



277 3.2.2 Faulting events of TA Trench

278 The trench TA exposed eight normal fault strands, at the hanging wall of the main bedrock fault plane, arranged both as
279 synthetic (Faults FA, FB, FC, FE, FF, and FG, in Fig. 5) and antithetic (Faults FD, in Fig. 5) splays to the main fault. The
280 fault FA was in the westernmost portion of the trench (Fig. 6) and displaced the youngest units of the stratigraphic
281 sequence. Based on the exposed stratigraphy and the structural relations observed on the trench walls, we determined
282 several faulting events from the displacement of different deposits and filled coseismic fissures.

283 On both trench walls, a well-expressed ~60-cm-wide sub-vertical fault zone associated with FA has placed in contact units
284 U3-U4-U5, to the east, with U5-U6-U7, to the west. These units were involved in the fault zone where there was evidence
285 of a back-tilting of the hanging wall units in the northern wall and of the footwall units in the southern wall, along the main
286 50° SW-dipping bedrock fault plane (Fig. 6). Moreover, at the hanging wall of FA, unit U5 incorporated an elongated
287 carbonate block with a long axis of around 50 cm, having an attitude parallel to the fault plane (the white clast drawn in the
288 lower part of the log of the southern wall; Fig. 6). The FA faulting events have determined the formation of fractures that
289 experienced different episodes of opening and subsequent infilling with the collapse of the involved deposits: on the
290 northern wall, the fracture walls defined a funnel shape widening from 25 cm at the base to 50 cm at the top of the exposure;
291 on the southern wall, the fractures had a complex wedge shape tapering downward and merging with the fault FA.

292 A noteworthy aspect of the stratigraphic setting uncovered by trench TA is that a large carbonate boulder was unearthed
293 during the excavation, right along the FA shear zone (Fig. 6). The boulder was a little less than a meter long, some tens of
294 centimetres large, and up to ten centimetres thick, the attitude of the long axis defined a roughly vertical position, paralleling
295 the fault zone. The considerable size of the block, the distance from the carbonate bedrock fault scarp (about 15 m apart),
296 the position right in the fault zone of FA, and the attitude (parallel to the fault plane) suggested that it might have been
297 intentionally placed there maybe by anthropic activities aimed at managing this part of the slope (i.e., creating stable
298 terraces for agricultural practices) owing to the presence of a (newly formed?) scarp. An alternative but much less probable
299 hypothesis is that the boulder fell from the carbonate scarp, rolled/bounced downslope and halted almost vertically right
300 on the FA shear zone, with the same attitude as the fault scarp. Unfortunately, the boulder has been accidentally removed
301 during the excavation of the trench, so we were not able to define accurately the relationship with the stratigraphic
302 sequence. Nonetheless, we can testify that it was at the contact between the below described Fi4 and Fi3 units and U3.

303 As for the fault FA, at least 4 faulting events have been identified since the deposition of unit U6 (plus an undefined number
304 of preceding faulting events mostly affecting the older U3, U4 and U5 units), whose succession has been reconstructed in
305 Fig. 7. The layers corresponding to units from U3 to U6 constituted the oldest exposed sediment involved in the FA faulting
306 and recording prior displacement events (Fig. 7a). The units U3-U6 were faulted by event Eq4, fissured, and displaced
307 vertically (Fig. 7b). The opening occurred was a maximum of 60 cm large, and the filling had a height of 70 cm. The infilling
308 deposit was unit Fi4, composed of a mixed deposit of U5-U6. At the end of this stage (Fig. 7c), the near vertical free face
309 was removed during the erosional phase that produced ES1, and a debris-facies colluvium (U7) deposition took place
310 subsequently (Fig. 7d). Unit U7 sealed the open fissure, constituting the wash-facies colluvium, and post-dated the first
311 surface rupture observed, Eq4. After unit U7, the deposition of unit U8 occurred but the following erosional processes
312 prevented its preservation (Fig. 7e).

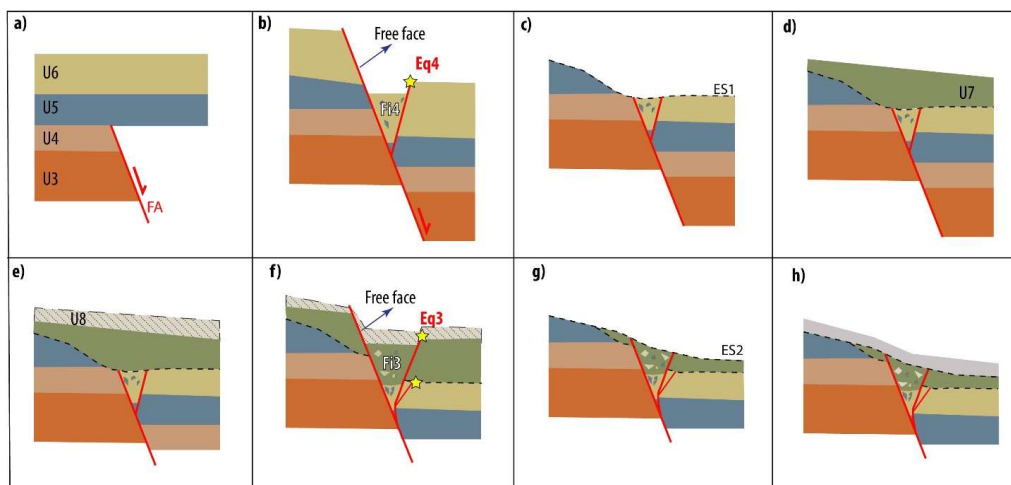
313 With earthquake Eq3, U7 and U8 were faulted (Fig. 7f). The fissure formed consequently to Eq3 was infilled by sediment
314 Fi3 from the immediate hanging wall and footwall, hence by a mix of U5-U6-U7-U8 deposits (Fig. 7g). By assuming the
315 same faulting events occurred on the two trench walls, we hypothesized the occurrence of two subsequent events. The
316 Fi2 deposit suggested the occurrence of Event Eq2 because its base unconformably overlays Fi3 s (Fig. 6). Moreover, the
317 evident triangular shape of Fi2 (inset in Fig. 6), and the proximity with fault FA suggests that it represents a colluvial wedge
318 formed after the event Eq2 owing to erosion of the coseismic surface scarp along FA. The thickness of the colluvial wedge
319 is 18 cm, and then the Eq2 event produced a minimum displacement of 36 cm (McCalpin, 2009).

320 The upslope limit of the colluvial wedge Fi2 coincides with the fault FA (Fig. 6). Specifically, the contact between Fi2, in
321 the FA hanging wall and U5, in the FA footwall, appears vertical and sharp. This suggests that the colluvial wedge Fi2 has



322 been cut once again by FA and placed in lateral contact with U5. Otherwise, one would expect that Fi2 has just
 323 unconformably overlaid U5, being the product of the fault footwall erosion. Instead, the abrupt lateral contact between Fi2
 324 and U5 was represented by the FA plane. This hence suggests a further episode of activation of the fault, which we name
 325 Eq1, that occurred after the deposition of Fi2 and that displaced Fi2 itself.

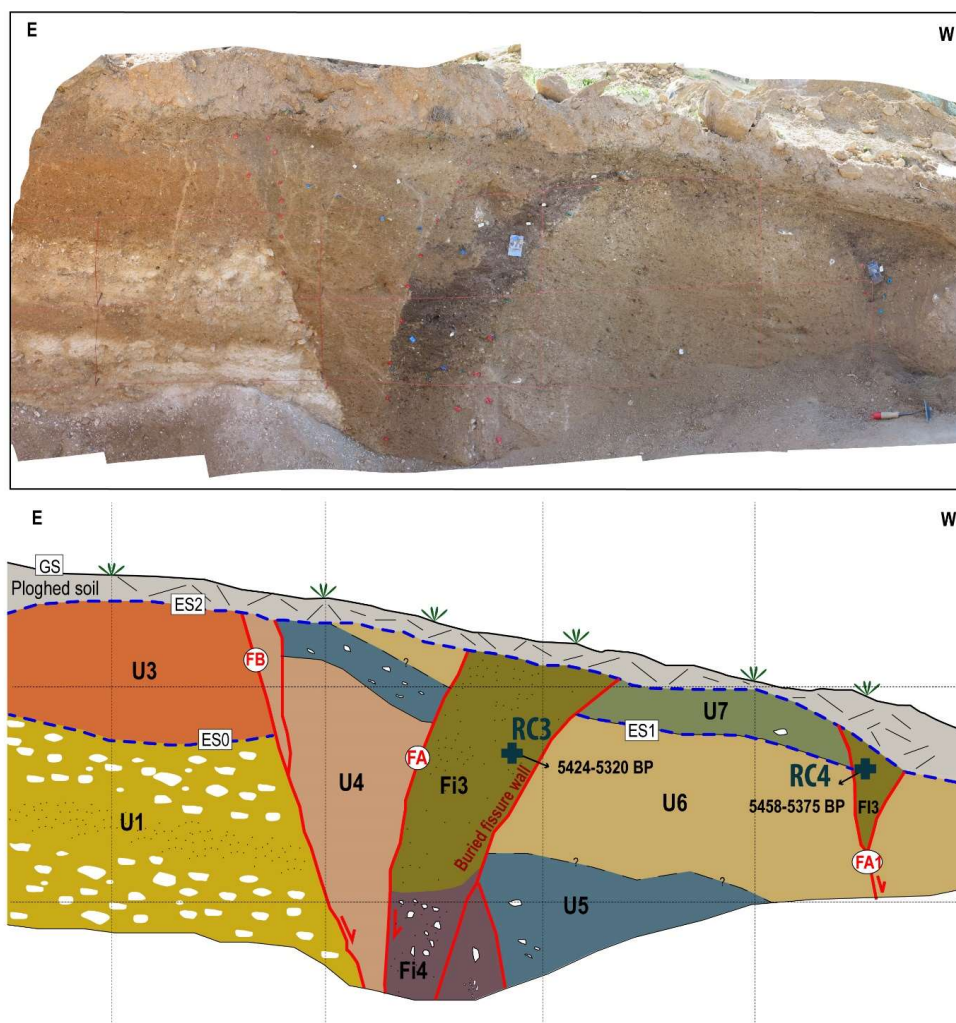
326 Due to human ploughing activities, a recent extended erosional process ES2 did not permit the maintenance of the first centimetres
 327 of the most recent stratigraphic succession (Fig. 7g), preventing the accurate determination of the thickness of the youngest units
 328 and then the paleo-event displacement measurements. Nevertheless, if we consider the best-preserved unit U5 outcropping on the
 329 northern wall of TA, the minimum thickness of U5 is 50 cm at the footwall and 100 cm at the hanging wall (see Fig. 6). Based on the
 330 displaced U5-U6 stratigraphic boundary, we estimated a cumulated minimum offset of ~140 cm associated with the fault FA
 331 (Fig. 7h). This minimum offset should be considered a cumulative of the 4 events.



332
 333 **Figure 7.** (a-h) Cartoons showing the structural and stratigraphic development of the exposures of the southern wall of
 334 Trench TA at the FA fault zone (Fig. 6). These cartoons assume that the stratigraphy before U5 was pre-faulted, and the
 335 fissure was developed and infilled following the earthquake faulting events, Eq4 and Eq3 (yellow stars).

336 3.2.3 Faulting events of TB Trench

337 The trench TB exposes the same stratigraphy of trench TA (Figg. 5 and 6), having at the base a well-stratified slope deposit
 338 (unit U1) directly lying under unit U3 (Figure 8). Unit U1 comprises carbonate stratified fan gravels containing orange,
 339 sandy levels 20 cm-thick dipping 15°. The more recent stratigraphic sequence fits well the observation of the units of the
 340 trench TA, except for unit U2, which is not present as it is localized only in the upper part of trench TA, close to the bedrock
 341 fault plane. Based on the identified stratigraphic contact, units U4-U5-U6-U7 have thicknesses of 100 cm, 20-60 cm, 90-
 342 100 cm, and 20-30 cm, respectively.



343

344 **Figure 8.** Above: orthophoto mosaic of the southern wall of trench TB, from Agisoft Photoscan. Below: stratigraphic log of
 345 the wall. Unit names and faults are indicated in the figure and referred to in Table 1. ES: erosional surface; GS: ground
 346 surface. The samples' position is indicated with a blue cross. The grid is each 100 cm.

347 The trench TB exposed three normal faults arranged synthetic to the principal Mt. Morrone Fault. The fault FB is defined
 348 by the contact of units U1-U3 at the footwall with units U4-U5 at the hanging wall, which allows its high-angle geometry
 349 recognition. The normal fault FA is instead defined by a nearly vertical, slightly E-dipping, pseudo-reverse fault and is also
 350 related to a buried fissure that shows a maximum opening of 65-70 cm, extending for the entire outcrop of the trench (160
 351 cm height).

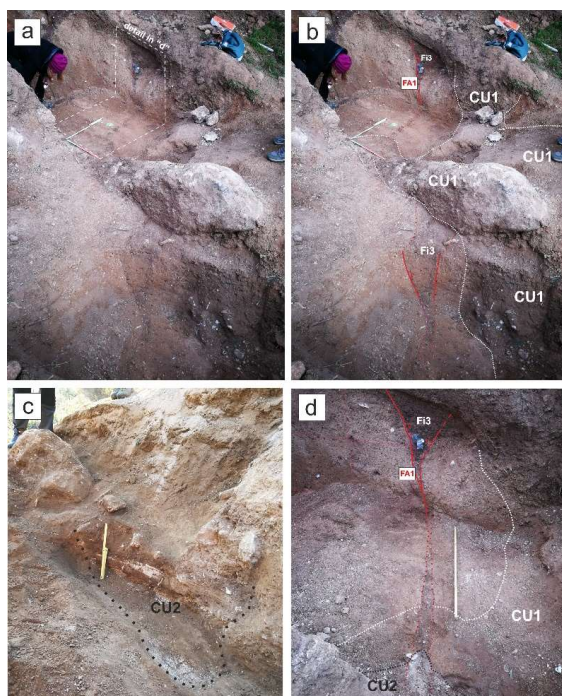
352 The arrangement of the material that filled the fissures suggests collapse material coming from hanging walls and/or
 353 footwall blocks. Similarly, to the trench TA, the infilling material is composed of two sediment types, respectively related to
 354 different displacement events. The Fi4 fracture infilling related to the Eq4 event is grey silty sand with the presence of 1
 355 cm-clasts diminishing upward, whereas Fi3, related to the Eq3 event, is composed by the units U6-U7 as parent material
 356 and by a 20 cm thick band of dark-brownish organic material bordering the outer wall of the fissure and filling the central
 357 portion. This band suggests the erosion of a paleosol previously overlying the U7 unit located both in the footwall and in



358 the hanging wall block of this fault, i.e., the unit U8 mentioned in the discussion of the TA trench. The southern TB trench
359 wall (Fig. 8) shows a well-developed open fissure 60 cm wide, suggesting that Eq3 has been a significant event in terms
360 of surface faulting. Fi3 appeared faulted along FA, as testified by the sharp and almost vertical contact with U4. If Fi3 had
361 not been faulted again along FA, the upslope flank of the large fracture infilled by Fi3 would have been smoothed and
362 upward convex, due to the erosion of the flank of the fracture, with a geometry comparable to its downslope flank (named
363 as "buried fissure wall" in Fig. 8). Lastly, the southern wall of trench TB displays a secondary fault FA1, located 150 cm
364 basinward from FA. It is defined by a 50 cm deep fissure, filled by dark sediments (presumably the same as unit Fi3, i.e.,
365 unit U8). The entire sequence is truncated at the top by the anthropogenic erosional surface (ES2) and sealed by the thin-
366 ploughed soil.

367 *3.3.2 Evidence of ancient human activities from Trench TB*

368 Further evidence collected within Trench TB corroborates ancient human activities along this sector of the Mt. Morrone
369 slope, as suggested by the above-mentioned boulder found juxtaposed on the FA scarp (see Fig. 6). At the western end
370 of trench TB, huge rock masses roughly superposed to one another were found during the excavation, the biggest of which
371 was more than 1 meter long and about 0.5 m large and thick. A dark brownish sandy matrix surrounded the boulders (Fig.
372 9a). The boulders and the matrix were filling an ancient excavation cut into unit 6, thus representing a cultural unit
373 (henceforth named CU1; Fig. 9b). (Fig. 9b... ex-9c). We then proceeded by archaeological-like stratigraphic investigation,
374 that is, by removing gradually each layer to investigate the vertical and horizontal relationship between the cultural unit and
375 the natural ones. This allowed us to achieve more constraints for the stratigraphy and, hence, for the fault activity (see Gori
376 et al., 2017 about these stratigraphic investigations for paleoseismological analyses). We found evidence that CU1 was
377 overlaid and crosscut by a younger cultural unit, henceforth named CU2 (Figg. 9c and d), that was made by a layered
378 deposit of alternating few cm-thick beds of well-sorted, clast-supported fine carbonate gravel and brownish sandy layers.
379 This unit filled a further ancient excavation made within CU1 (Fig. 9c). Such archaeological-like investigations allowed us
380 to unravel the relationship between the two uncovered cultural units and the fault planes exposed along the trench walls.
381 As shown in Fig. 9b, CU1 is superimposed to the Fi3 infilling of the secondary fracture related to FA1 (Fig. 9d)) meaning
382 that CU1 was "settled" after the occurrence of Eq3. In turn, both CU1 and CU2 were affected by another event of activation
383 of FA1, as the continuity of the CU1 boundary is interrupted by the fracture and the materials of CU2 partly fill the void
384 which formed with the displacement along FA1 (Fig. 9d).



385

386 **Figure 9.** a) SW end of trench TB, where two anthropic units CU1 and CU2 were found. b) fault planes FA1 (red lines) that
387 displaced the natural and cultural units; the boundaries of unit CU1 are marked by a white dotted line. c) close-up view of
388 cultural unit CU2, whose limits are outlined by the black dotted line. d) close-up view of the southern portion of the SE wall
389 of trench TB that shows the relationship between the fault, the natural and cultural units; CU1 cross-cuts the former fracture
390 formed along FA1 but the fault plane and associated fracture (red lines) have displaced the cultural units CU1 and CU2
391 during an activation event of FA1 subsequent to CU2 deposition; the boundaries of units CU1 and CU2 are marked by
392 white and black dotted lines, respectively.

393 In terms of chronology, archaeological investigations made in the past decades revealed human presence along this sector
394 of the Mt. Morrone SW slope since at least the Bronze Age. Within this light, just upslope of the trenching site,
395 archaeological remnants of an ancient, fortified settlement of local pre-Roman, Italic populations were already well-known.
396 These are represented by traces of ancient walls made of polygonal masonry that bounds the top of a relief known as
397 “Colle delle Fate”. This fortified settlement belongs to a series of fortified sites found in this part of the central Apennine
398 and aged in 7th-4th century BCE, likely around the 4th century BCE, when such fortified structures represented the pivotal
399 centres for the territorial organisation and management in the late pre-Roman age (Mattiocco, 1981; Van Wonterghem,
400 1984). Although we could not discriminate which period the unearthed cultural units belong to, we can stress that they can
401 be attributed to a period not earlier than the Bronze Age.

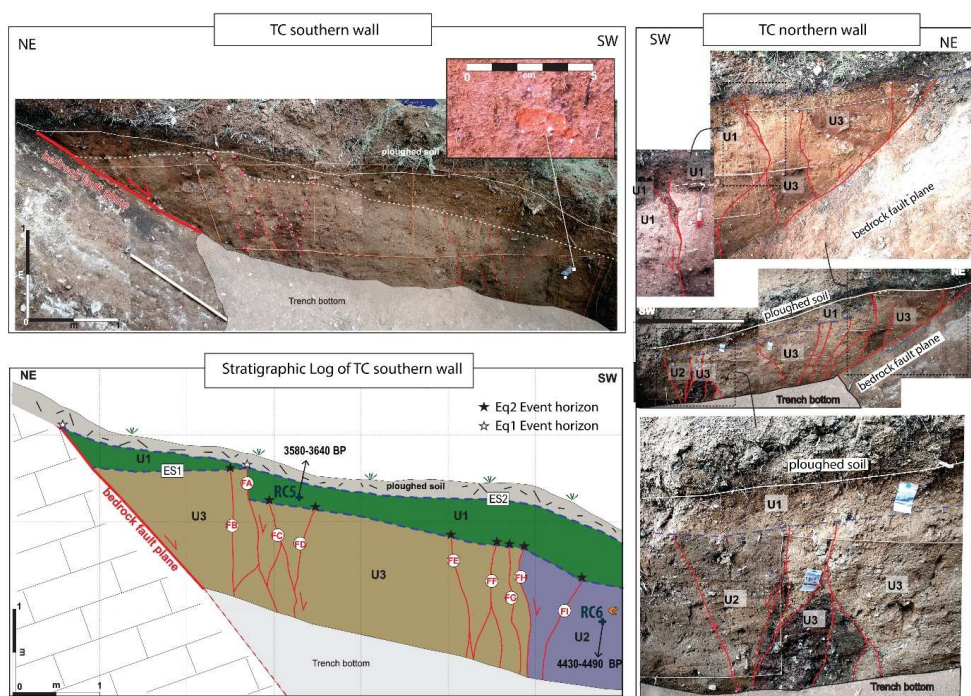
402 3.3 The TC and TD trenches

403 3.3.1. Stratigraphic setting of TC and TD

404 The excavations of the two further trenches TC and TD revealed a stratigraphic sequence different from that in trenches
405 TA and TB. It was made by a series of colluvial deposits that we distinguished from one another by the abundance of
406 carbonate clasts, the quantity of clay in the matrix, and the colour of the matrix itself. We distinguished three main units
407 (from the youngest to the oldest: Unit U1, Unit U2 and Unit U3). Unit U3 was made by different colluvial bodies that



408 experienced intense deformation induced by fault activity, causing local mixing that hindered a more detailed stratigraphic
 409 distinction.
 410 Two charcoal shards collected in U2 and U1 provided radiocarbon ages of 4460 ± 30 yr BP and 3610 ± 30 yr BP, respectively
 411 (RC5 and RC6 in Table 1), thus testifying to the late Holocene age of the youngest stratigraphic sequence exposed. The
 412 very recent age of the sequence is also confirmed by the presence of a pottery shard in unit U2, whose size and state of
 413 preservation hindered archaeological determination (Fig. 10).
 414 In trench TD, the erosional surface ES2, which in trench TC separated U1 from the cultivated soil, cut through the whole
 415 stratigraphic sequence, removing almost wholly U1. Only a tiny portion of U1 remained, so the ploughed ground directly
 416 overlaid unit U3 along most of the trench (Fig. 11).
 417



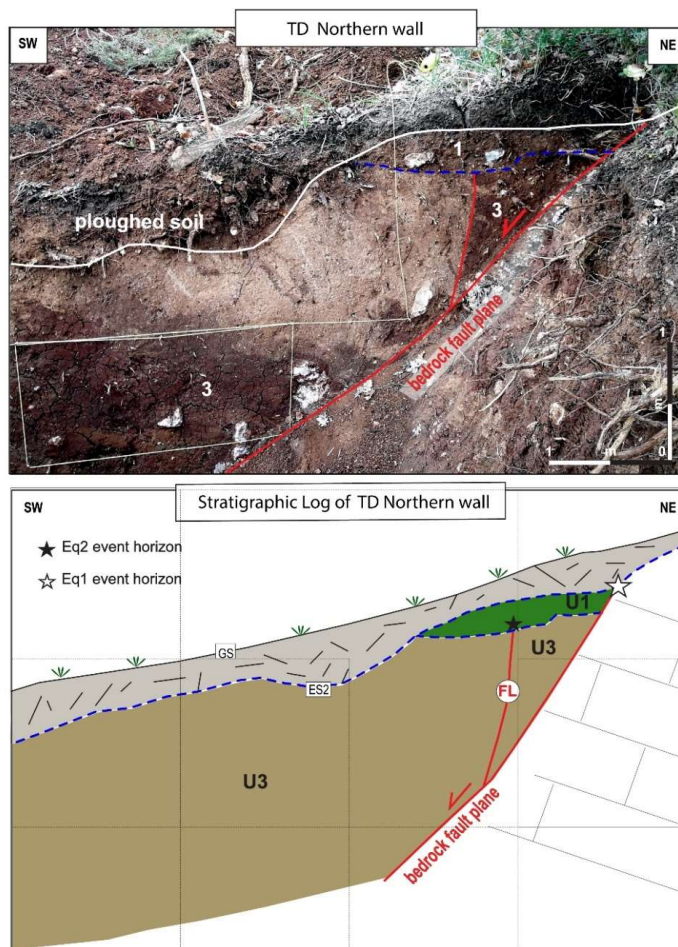
418
 419 **Figure 10.** Left: Picture of the southern wall of trench TC (upper panel) and related stratigraphic log scheme (lower panel);
 420 red lines mark the fault planes. Stratigraphic units 1, 2 and 3: colluvial units, made of carbonate angular clasts in a sandy
 421 and sandy-clayey, brownish, greyish, and yellowish matrix. The pottery shard found within unit U2 is shown in the inset.
 422 Right: Picture of the northern wall of trench TC. The stratigraphic units are the same as the southern wall; red lines mark
 423 the fault planes. In the middle and lower panels close-up views of the fault zones. ES: erosional Surface; GS: Ground
 424 Surface. The sample's position is indicated with a light blue cross.

425 3.3.2 Faulting events of TC and TD

426 Except for the ploughed soil, all units were displaced and deformed by the main fault plane and by a set of synthetic and
 427 antithetic faults (Fig.s 10 and 11). The relationship between the stratigraphic sequence and the fault planes revealed at
 428 least two faulting events. The oldest one was responsible for displacing units U3 and U2, placed in contact by fault FH.
 429 The event occurred before the deposition of Unit U1, which sealed the faulting event. The youngest event displaced Unit



430 U1 along the main bedrock fault plane and fault FA and caused a minimum offset of unit U1 of about 1 m in trench TC (Fig.
431 10). In trench TD, U1 was only displaced by the main fault plane with a minimum offset of 15-20 cm.



432

433 **Figure 11.** Picture of the northern wall of trench TD (upper panel) and related stratigraphic log scheme (lower panel); red
434 lines mark the fault planes. The stratigraphic units are the same as described in Fig. 9. ES: erosional Surface; GS: Ground
435 Surface.

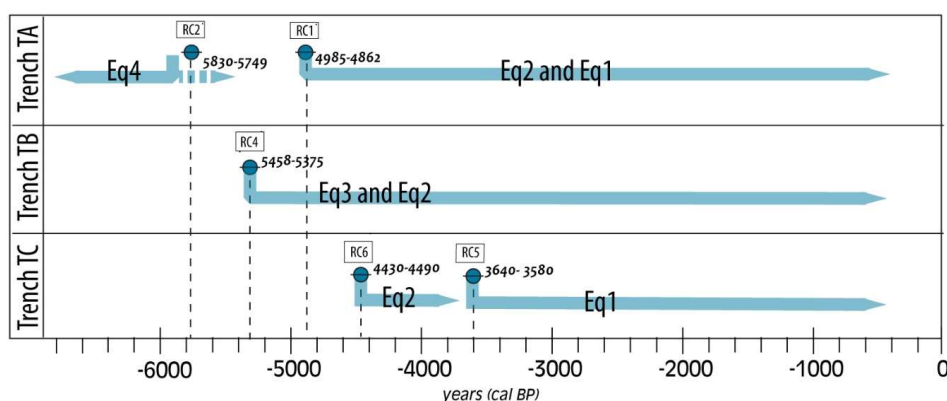
436 4 Discussion and Conclusion

437 Our paleoseismological study was performed south of Roccasale village, on the central portion of the Mt. Morrone fault,
438 showing that the basin-bounding fault is a fault with evidence of activity during the Late Pleistocene-Holocene. The
439 paleoseismic study highlighted a 15 m-wide zone of deformation associated with two primary fault zones: the bedrock fault
440 plane zone, and a fault zone corresponding to a morphological fault scarp, related to synthetic and antithetic faults'
441 branches. The fault scarp involves late Holocene colluvial deposits and records at least 4 fault activation events associated
442 with as many surfaces rupturing seismic events along the MMF.



443 **4.1 Evidence and timing of past earthquakes**

444 The bulk of the observations we made in the trenches allowed us to define the most recent events of activation of the fault.
 445 Based on the available age constraints correlated among the four trenches, analyzing the stratigraphic sequences and
 446 utilizing the radiocarbon dating as the "terminus post quem" (that is, charcoal fragments or organic matter dated are
 447 contained within or are the matrix of detrital colluvial/slope-derived sediments, thus implying that the age obtained is not
 448 the age of deposition of the stratigraphic unit, but it predates sedimentation), the occurrence of the four identified faulting
 449 events can be defined (Fig. 12).



450

451 **Figure 12.** Chronogram of the surface-rupture events identified from within the TA-TB-TC trenches. Each radiocarbon
 452 sample is indicated by the blue circle, labelled, and reported with its 2σ calibrated interval. Horizontal blue arrows point to
 453 the assumed paleo event age of occurrence as deduced from the post-quem samples age (see text for further details).

454 The oldest earthquake faulting event Eq4 was observed in the Trench TA and, according to the interpretation of the event
 455 horizon, it predates the emplacement of unit U7. Unit U7 is a colluvial deposit, associated with vertical free-face dismantling;
 456 the charcoal embedded in the deposit provides a date of the U7 deposition after 5830-5749 yr BP. Therefore, although we
 457 do not have chronological constraints of the Eq4 event, we can affirm that the oldest event horizon is sealed by colluvium
 458 deposited after 5.8 ± 0.4 Kyr BP. As highlighted before, the age of the charcoal in the colluvial unit is not the age of the
 459 deposition but it predates the deposition.

460 The Eq3 event is observed both in the trenches TA and TB (see Figs. 6 and 8) and its chronology was constrained by
 461 dating charcoals on the trench TB. The ages of the organic material filling the two fissures related to the faults FA and FA1
 462 (trench TB, Fig. 8) are comparable (5458-5375 yrs BP and 5424-5320 yrs BP, respectively), and both confirm the
 463 contemporaneous occurrence of Eq3 event after this age. The Eq2 event is observed on the trench TA by the colluvial
 464 wedge Fi2 and on the trench TC by the faulting evidence of unit U2. Considering the charcoal dating more reliable than
 465 the bulk age, the best constraint of event Eq2 has been retrieved by dating the charcoal from unit U2 of the trench TC
 466 which testifies to the topography at the Eq2-time and provides a post-quem age for the penultimate Eq2 event of 4.4 ± 0.3
 467 kyr BP. The fact that FA1 affected the cultural units CA1 and CA2 (not earlier than the initial Bronze Age, i.e., about 3700-
 468 3600 BP in the central Apennines: e.g., Silvestri, 2016; section 3.3.2) corroborates the occurrence of a faulting event after
 469 Eq3 that re-activated the fault FA1.

470 The most recent event, Eq1, is observed in Trench TA (northern wall) by the faulted colluvial wedge (Fi2) and in Trench
 471 TC where its occurrence is testified by the displacement of unit U1, producing 1 m minimum surface displacement. The
 472 chronology of Eq1 can be retrieved by the charcoal found in the deposit of TC, which yielded an age of 3580-3640 yrs BP,
 473 defining that Eq1 occurred after this age. In summary, based on interpretations and dating from the four investigated



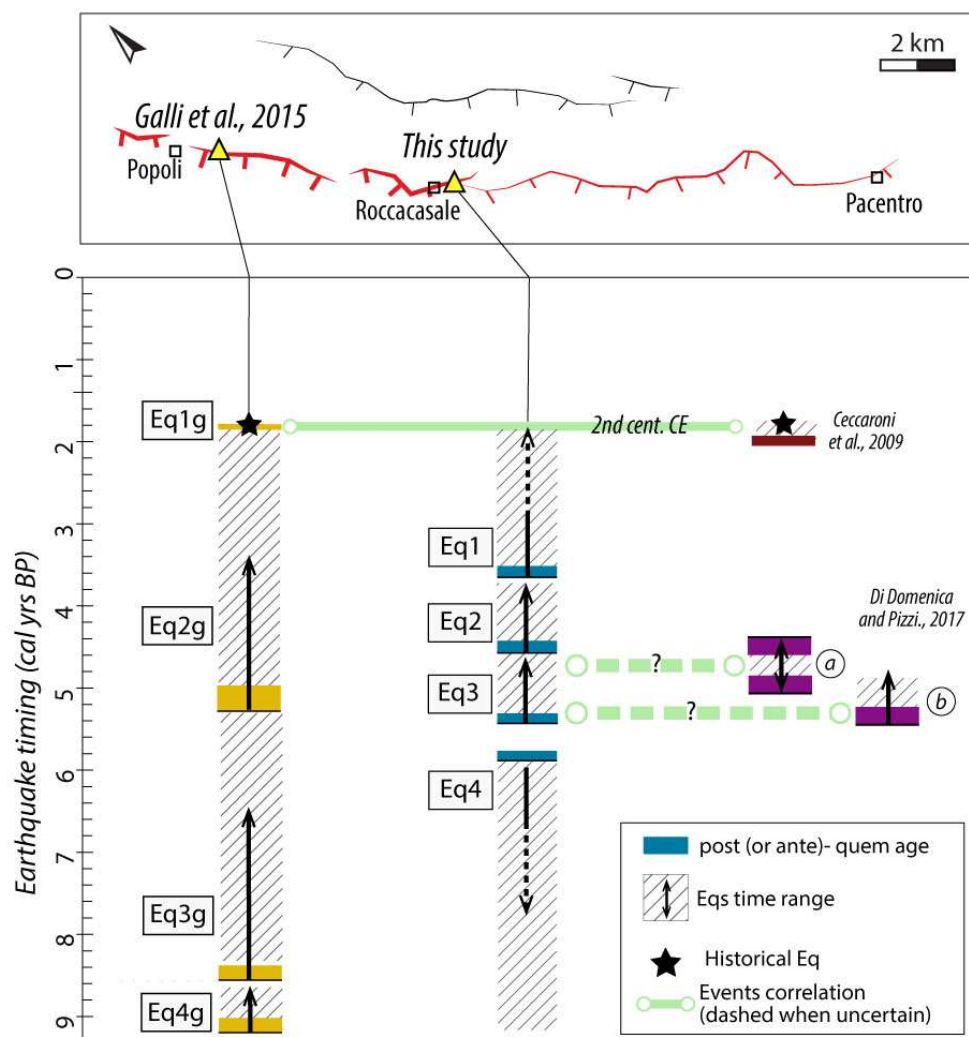
474 trenches, the basin-bounding fault of the MMF has undergone at least three seismic events over the last approximately
475 5500 years.

476 *4.2 Comparison with previous paleoseismological investigation*

477 The comparison with the previous paleoseismological investigation of Galli et al. (2015), performed at the northern tip of
478 the fault (close to Popoli), allows a good time constraint of the events that occurred over the Holocene and provides a well-
479 defined scenario of the rupturing occurrence along the basin-bounding fault. All the paleoseismological investigations, both
480 ours and Galli's and co-authors' ones, have been performed on the Sulmona basin-bounding fault, i.e., the western splay
481 of the MMF System. The four trenches of Popoli have shown the presence of a fault offsetting Quaternary deposits and
482 recording, overall, four events over the last ~9000 yrs BP (Fig. 13).

483

484



485 **Figure 13.** Chronogram of the surface-rupture events for the MMF. In the panel events from dating in literature are reported:
 486 yellow from Galli et al. (2015), purple from Di Domenica and Pizzi (2017) and red from Ceccaroni et al. (2009). The two
 487 age intervals from Di Domenica and Pizzi (2017) are from a) speleothems radiocarbon dating (i.e., ante and post quem
 488 termini) and b) radiocarbon dating of wood embedded in a rock avalanche (see the main text for further details). Data from
 489 this study is indicated in blue. Each coloured rectangle is a radiocarbon sample, and the height reports its 2σ calibrated
 490 interval of age. Black arrows indicate the range of the event occurrence constrained by the post-quem data. The striped
 491 rectangles indicate the range of time-occurrence uncertainty related to each event. Green lines indicate the events
 492 correlations (dashed when hypothesized because not directly correlated to on-fault data).

493 **The authors** reported the ultimate event (Eq1g) in ~ 2000 yrs BP, corresponding to the 2nd century CE earthquake, also
 494 individuated by the former archaeoseismological investigations (Galadini and Galli, 2001; Ceccaroni et al., 2009). In the
 495 present study, the ultimate detected event (Eq1) has been recognized in the trenches TA and TC of Roccasale, which
 496 constrained the event after 3610 ± 30 yrs BP. Such event produced a minimum recorded vertical displacement of 1 m,
 497 suggesting an activation of the entire fault, able to produce widespread damages to villages, like those
 498 archaeoseismologically inferred (Ceccaroni et al.; 2009).



499 The penultimate event was observed at the Popoli trenches where Galli et al. (2015) estimated 185 cm of vertical
500 displacement (Eq2g). The occurrence of the paleoearthquake was found after 5280-4970 yrs BP, determined by detrital
501 charcoal in colluvial units right below the coseismic fissure. In our trenches, the penultimate event Eq2 has been identified
502 with an age post of 4490-4430 yrs BP, and so it shows a shorter time window than the Popoli site Eq2g event. The lack of
503 a well-constrained slip per event on the Roccacasale site prevents the comparison in terms of displacements between the
504 two penultimate events (Eq2g and Eq2); hence, two open hypotheses can be made for the comparison between the trench
505 sites. The first hypothesis is to consider Eq2g the same as Eq2 so that the coseismic throw of 36 cm retrieved in the
506 Roccacasale should be considered a minimum. The second scenario is that the Eq2 is an event not observed in the Popoli
507 trenches due to *i*) the not recording in the investigated trenches, or *ii*) the lack of coseismic faulting at the northern MMF
508 sector (so that, the low vertical displacement recorded **on the trench** may indicate an event with magnitude lower than the
509 Eq1). In this case, the Eq2g would correspond to the third-ultimate event recognized in the Roccacasale site, the Eq3
510 dated post 5458-5375 yrs BP. At the Roccacasale site, we retrieved an opening fissure measurement of 70 cm related to
511 the Eq3 event, which is comparable to the opening values observed in the Popoli site (100 cm). Considering the similar
512 topographic conditions of the two sites, such close opening values might suggest the occurrence of the same triggering
513 event in terms of magnitude indeed. Thus, the Eq3 event should reasonably correspond to the Eq2g, and then it can be
514 an event that occurred after 5280-4970 yr BP.

515 Moreover, speleo-seismological studies around 10 km conducted to the East of the MMF, by Di Domenica and Pizzi (2017)
516 in the Cavallone cave (close to the Majella Massif, see Fig. 1) revealed the occurrence of a seismic-induced gravitational
517 collapse of stalagmites in the cave, whose age was constrained between 4815-4755 and 4675-4645 yr BP. Again, the
518 authors dated a well-preserved buried wood (the portion of a *Quercus ilex* trunk) incorporated within a seismic-induced
519 landslide body, close to the Palena village, corresponding with an age of 5445-5300 yr BP. Although the authors did not
520 **assess for certain the simultaneous occurrence** of these two events, the comparable age range of these exceptional and
521 catastrophic events suggests that both the cave damage and the rock avalanche may represent the effects of strong
522 paleoearthquakes. The collapse of the speleothem suggests the occurrence of a strong earthquake between 4.8-4.6 kyr
523 BP in the region, but not necessarily associated with the MMF activation. On the other hand, the chronological constraints
524 related to the Palena rock avalanche indicate an event occurred after 5.4-5.3 kyr BP, that results in good agreement with
525 the chronologies of the Eq3 event retrieved by our paleoseismological study. Furthermore, paleoseismological evidence
526 of the ruptures might also indicate the occurrence of a **local event stronger than 6.5**, caused by a larger seismogenic source
527 of the region. Within this light it must be underlined that this part of the Maiella massif in which the speleothems' collapse
528 was founded, has been affected by the 1706 earthquake ($M \sim 6.8$), whose seismogenic source is still undefined, and
529 tentatively associated with a reverse structure (De Nardis et al., 2008; Galli et al. 2019).

530 By dating the organic materials found directly below a colluvial wedge on the Popoli trenches, it was determined that a
531 third event Eq3g occurred after 8540-8370 years BP. The Eq4 observed in our study can be compared to this event. Based
532 on our analysis of a charcoal sample from the colluvium (U7) that was deposited after Eq4 at 5830-5749 yr BP, we should
533 assume that Eq4 was an event that occurred before this age. Thus, it can agree with Eq3g. In the Popoli trenches, a final
534 event called Eq4g was observed and dated to after 9090-8980 years BP.

535 Overall, the new available chronological constraints of the four paleoearthquakes revealed by the Roccacasale trenches
536 along with the integration of the existing paleoseismological and archaeoseismological data (i.e., Galadini and Galli, 2001;
537 Ceccaroni et al., 2009; Galli et al., 2015; Di Domenica and Pizzi, 2017) allows a better definition of the Holocene behaviour
538 the MMF. By matching the observations and combining the evidence from the literature, the last fault activation we identified
539 is consistent with the most recent event in the 2nd century CE (Eq1) defined by previous studies, the penultimate event
540 occurred after 4.4 kyr BP (Eq2), a third-ultimate event took place after 5.4-5.3 kyr (Eq3; between 4.8 kyr and 4.6 kyr BP, if
541 coincident with the cave's collapse), and the last event occurred presumably before 5.8-5.7 kyr BP and after 8.5-8.4 kyr
542 BP.



543 Considering the evaluated constraints for the faulting events, we defined an average recurrence time for characteristic
544 earthquakes by considering the last three events that occurred over the last 5.4 kyr (for which we identified a post-*quem*
545 age). By dividing this interval by the three events (i.e., Eq3, Eq2 and Eq1) we determined an average recurrence interval
546 of 1800 yrs for M6.5-7-like events). This result agrees with the average recurrence time in the Central Apennines (Galadini
547 and Galli, 2000). On the other hand, preceding studies show the occurrence of four events over the last 9 kyr, and suggest an
548 average recurrence interval of 2400 yrs (Galli et al., 2015). Therefore, considering that the elapsed time since the last event Eq1
549 is ~1850 yrs (which recorded at both sites a minimum displacement of 1 m), the newly determined recurrence interval has
550 important implications as it reveals that the fault might be closer to failure. Therefore, the new data should be carefully considered
551 and included in the estimations of the Central Italy probability of earthquake occurrence.

552 In conclusion, this study corroborates the findings available in the literature, while refining and extending the chronological
553 record of the paleoseismic history of the MMF, particularly for the past 5000-6000 years. This is a crucial aspect for
554 assessing earthquake probability in the central Apennines. In this context, the MMF is considered a "silent" active and
555 seismogenic fault (Galadini and Galli, 2000), meaning that it represents a major tectonic structure of which the elapsed
556 time since the last activation approximates the fault's recurrence interval. Specifically, our results have shortened the
557 previously defined mean recurrence interval of the MMF to approximately 1800 years, which corresponds to the time
558 elapsed since its last activation. In this context, the 2016 seismic sequence in central Italy is worth mentioning. Prior to
559 2016, the Mt. Vettore-Bove fault was deemed as a major active seismogenic fault in the central Apennines, potentially
560 responsible for M 6.5-6.6 earthquakes (based on geological and paleoseismological studies), and it was also considered
561 "silent" (Galadini and Galli, 2003), similar to other active faults in the central Apennines, including the MMF. The 2016
562 seismic sequence confirmed this hypothesis, as it was caused by the activation of the Mt. Vettore-Bove fault, which fully
563 ruptured, generating three major seismic events, the strongest of which occurred on October 30, 2016, with a magnitude
564 of M_w 6.5 (e.g. Chiaraluce et al., 2017; Cheloni et al., 2019; Civico et al., 2018).

565 The 2016 central Italy seismic sequence thus demonstrated the reliability, efficacy, and necessity of this kind of studies on
566 active faults, which are primarily based on thorough geological investigations aimed at defining fault activity over long
567 timespans (from tens to hundreds of thousands of years), and then detailed paleoseismological analyses aimed at
568 understanding fault behaviour over the past few thousand years. This is particularly significant in areas like the central
569 Apennines, where numerous towns, inhabited by thousands of people, are located, encompassing cultural heritage and
570 productive activities. Regarding the MMF, its potential to produce strong seismic events (with magnitudes of up to 6.5-7;
571 Bordoni et al., 2023), coupled with the absence of recent historical earthquakes and the newly defined average recurrence
572 interval, confirms it as one of the most problematic active tectonic structures in this part of Italy.

573 ACKNOWLEDGEMENTS

574 This work has been funded by the Italian Ministry for Education, University and Research (MIUR) (ex 60% grants to A.
575 Pizzi). Public funds from the Municipality of Roccasale also supported this work. The 2018 mayor of Roccasale, Enrico
576 Pace, is acknowledged for his interest in scientific study. A special thanks to geologists Mimmo Trotta, Catia Di Nisio, and
577 Tania Campea, who are recognised for their support and help in the field and logistics.

578
579 **Competing Interests:** The authors declare that they have no known competing financial interests or personal
580 relationships that could have appeared to influence the work reported in this paper.

581 **Author Contributions:** Conceptualization, A.P.; Data Acquisition and Field analysis, I.P., A. P., S.G., E. F., M. M.,
582 M. S. and F.G.; Data Curation, I.P., S.G. and E.F.; Figures production, I.P. and S.G.; GIS mapping and Writing—Original
583 Draft Preparation, I.P., S.G. and E.F.; Supervision and Project administration, A.P. and F.G.; Funding Acquisition, A.P. and
584 F.G.



585 REFERENCES

- 586 Benedetti, L., Manighetti, I., Gaudemer, Y., Finkel, R., Malavieille, J., Pou, K., Arnold, M., Aumaître, G., Bourlès, D., and Keddadouche,
587 K. (2013). Earthquake synchrony and clustering on Fucino faults (Central Italy) as revealed from in situ³⁶Cl exposure dating. *Journal*
588 *of Geophysical Research: Solid Earth*, 118(9), 4948–4974. <https://doi.org/10.1002/jgrb.50299>
- 589 Benvenuti, M., and Martini, I. P. (2009). Analysis of Terrestrial Hyperconcentrated Flows and their Deposit. *Flood and Megaflood*
590 *Processes and Deposits*, 167–193. <https://doi.org/10.1002/9781444304299.ch10>
- 591 Boccaletti, M., Ciaranfi, N., Cosentino, D., Deiana, G., Gelati, R., Lentini, F., Massari, F., Moratti, G., Pescatore, T., Ricci Lucchi, F., and
592 Tortorici, L. (1990). Palinspastic restoration and paleogeographic reconstruction of the peri-Tyrrhenian area during the Neogene.
593 *Palaeogeography, Palaeoclimatology, Palaeoecology*, 77(1), 41–IN13. [https://doi.org/10.1016/0031-0182\(90\)90097-Q](https://doi.org/10.1016/0031-0182(90)90097-Q)
- 594 Bosi, C., and Bertini, T. (1970). *Geologia della Media Valle dell'Aterno*. In *Memorie della Società Geologica Italiana* (Vol. 9, pp. 719–777).
595 Calamita, F., and Pizzi, A. (1992). Tettonica quaternaria nella dorsale appenninica umbro-marchigiana e bacini intrappenninici associati.
596 <http://193.204.8.201:8080/jspui/handle/1336/541>
- 597 Bosi C., Galadini F., Giaccio B., Messina P. and Sposato A. (2003) -Plio-Quaternary continental deposits in the Latium-Abruzzi: the
598 correlation of geological events across different intermontane basins. *Il Quaternario*, 16, 55-76.
- 599 Carrara, C. (1998). I travertini della Valle del Pescara tra Popoli e Tor de' Passeri (Abruzzo, Italia Centrale). In *Alpine and Mediterranean*
600 *Quaternary* (Vol. 11, Issue 2, pp. 163–178).
- 601 Cavinato, G. P., and MICCADEI, E. (2000). Pleistocene carbonate lacustrine deposits: Sulmona basin (central Apennines, Italy). *Lake*
602 *Basins through Space and Time*. *Am. Assoc. Pet. Geol. Stud. Geol*, 46(Figure 2), 517–526. [papers3://publication/uuid/2A028136-](https://doi.org/10.1002/10.1002/9781444304299.ch10)
603 [191F-41A8-9A9B-049E405CF63C](https://doi.org/10.1002/9781444304299.ch10)
- 604 Cavinato G.P. Cosentino D., D. R. D. F. R. and P. M. (1994). Tectonic-sedimentary evolution of intrapenninic basins and correlation with
605 the volcano-tectonic activity in Central Italy. In *Memorie Descrittive della Carta Geologica d'Italia*: Vol. XLIX (pp. 36–76).
- 606 Ceccaroni, E., Ameri, G., Gómez Capera, A. A., and Galadini, F. (2009). The 2nd century AD earthquake in central Italy:
607 Archaeoseismological data and seismotectonic implications. *Natural Hazards*, 50(2), 335–359. [https://doi.org/10.1007/s11069-009-](https://doi.org/10.1007/s11069-009-9343-x)
608 [9343-x](https://doi.org/10.1007/s11069-009-9343-x).
- 609 Cheloni D., Falcucci E., Gori S. (2019). Half-graben rupture geometry of the 30 October 2016 MW 6.6 Mt. Vettore-Mt. Bove earthquake,
610 central Italy. *Journal of Geophysical Research: Solid Earth*, 124. DOI: 10.1029/2018JB015851
- 611 Chiaraluze L., Di Stefano R., Tinti E., Scognamiglio L., Michele M., Casarotti E., Cattaneo M., De Gori P., Chiarabba C., Monachesi G.,
612 Lombardi A., Valoroso L., Latorre D., Marzorati S. (2017). The 2016 central Italy seismic sequence: a first look at the mainshocks,
613 aftershocks and source models. *Seismological Research Letters*, 88(3), 757–771. DOI: 10.1785/0220160221
- 614 Ciccacci, S., D'Alessandro, L., Dramis, F., and Miccadei, E. (1999). Geomorphologic evolution and neotectonics of the Sulmona
615 intramontane basin (Abruzzi Apennine, Central Italy). *Zeitschrift Fur Geomorphologie, Supplementband*, 118(November).
- 616 Cipollari, P., and Cosentino, D. (1995). Miocene unconformities in the Central Apennines: geodynamic significance and sedimentary basin
617 evolution. *Tectonophysics*, 252(1–4), 375–389. [https://doi.org/10.1016/0040-1951\(95\)00088-7](https://doi.org/10.1016/0040-1951(95)00088-7)
- 618 Cipollari, P., Cosentino, D., and Gliozzi, E. (1999). Extension- and compression-related basins in central Italy during the Messinian Lago-
619 Mare event. *Tectonophysics*, 315(1–4), 163–185. [https://doi.org/10.1016/S0040-1951\(99\)00287-5](https://doi.org/10.1016/S0040-1951(99)00287-5)
- 620 Cipollari, P., Pipponzi, G., 2003. Le "Calciruditi di Calaturo" (Montagna del Morrone): un deposito tardo-orogénico della fine del Pliocene
621 inferiore. *Studi Geologici Camerti, Numero Speciale*, 1/2003. 73–83.
- 622 Civico, R., Pucci, S., Villani, F., Pizzimenti, L., De Martini, P. M., Nappi, R., & the Open EMERGEIO Working Group (2018). Surface
623 ruptures following the 30 October 2016 Mw 6.5 Norcia earthquake, central Italy. *Journal of Maps*, 14(2), 151–160.
624 <https://doi.org/10.1080/17445647.2018.1441756>.
- 625 De Nardis, R., Pace, B., Lavecchia, G., Visini, F., and Boncio, P. (2008, December). Geological and macroseismic data for seismotectonic
626 purpose: the 1706 Maiella (Abruzzo, Italy) earthquake case study. In *AGU Fall Meeting Abstracts* (Vol. 2008, pp. T21B-1946).
- 627 Di Domenica, A., and Pizzi, A. (2017). Defining a mid-Holocene earthquake through speleoseismological and independent data:
628 Implications for the outer Central Apennines (Italy) seismotectonic framework. *Solid Earth*, 8(1), 161–176. [https://doi.org/10.5194/se-](https://doi.org/10.5194/se-8-161-2017)
629 [8-161-2017](https://doi.org/10.5194/se-8-161-2017)
- 630 Doglioni, C. (1991). A proposal for the Kinematic modelling of W-dipping subductions - possible applications to the Tyrrhenian-
631 Apennines system.
- 632 Duross, C. B., Personius, S. F., Crone, A. J., Olig, S. S., and Lund, W. R. (2011). Integration of paleoseismic data from multiple sites to
633 develop an objective earthquake chronology: Application to the Weber segment of the Wasatch fault zone, Utah. *Bulletin of the*
634 *Seismological Society of America*, 101(6), 2765–2781. <https://doi.org/10.1785/0120110102>



- 635 Duroso, C., Olig, S. S., Lund, W. R., and Schwartz, D. P. (2016). Fault Segmentation: New Concepts from the Journal of Geophysical
636 Research: Solid Earth. November. <https://doi.org/10.1002/2015JB012519>
- 637 Ekström, G., Morelli, A., Boschi, E., and Dziewonski, A. M. (1998). Moment tensor analysis of the central Italy earthquake sequence of
638 September–October 1997. *Geophysical Research Letters*, 25(11), 1971–1974.
- 639 Falcucci, E., Gori, S., Moro, M., Pisani, A. R., Melini, D., Galadini, F., and Fredi, P. (2011). The 2009 L'Aquila earthquake (Italy): What's
640 next in the region? Hints from stress diffusion analysis and normal fault activity. *Earth and Planetary Science Letters*, 305(3–4), 350–
641 358. <https://doi.org/10.1016/j.epsl.2011.03.016>
- 642 Falcucci E, Gori S., Bignami C, Pietrantonio G, Melini D, Moro M, Saroli M, Galadini F (2018). The Campotosto seismic gap in between
643 the 2009 and 2016–2017 seismic sequences of Central Italy and the role of inherited lithospheric faults in regional seismotectonic
644 settings. *Tectonics*, 37, 2425–2445, <https://doi.org/10.1029/2017TC004844>.
- 645 Friedrich, A. M., Wernicke, B. P., Niemi, N. A., Bennett, R. A., and Davis, J. L. (2003). Comparison of geodetic and geologic data from the
646 Wasatch region, Utah, and implications for the spectral character of Earth deformation at periods of 10 to 10 million years. 108, 1–23.
647 <https://doi.org/10.1029/2001JB000682>
- 648 Galadini, F., and Galli, P. (2000). Active Tectonics in the Central Apennines (Italy) – Input Data for Seismic Hazard Assessment. *Natural
649 Hazards*, 22(3), 225–270. <https://doi.org/10.1023/A:1008149531980>
- 650 Galadini F., Galli P., 2001. Archaeoseismology in Italy: case studies and implications on long-term seismicity. *Journal of Earthquake
651 Engineering*, 5, 35–68.
- 652 Galadini, F., & Galli, P. (2003). Paleoseismology of silent faults in the Central Apennines (Italy): The Mt. Vettore and Laga Mts. faults.
653 *Annals of Geophysics*, 46(5), 815–836. <https://doi.org/10.4401/ag-3457>.
- 654 Galadini, F., Messina, P. (2004). Early-Middle Pleistocene eastward migration of the Abruzzi Apennine (central Italy) extensional domain.
655 *Journal of Geodynamics*, 37(1), 57–81. <https://doi.org/10.1016/j.jog.2003.10.002>
- 656 Galli, P., Galadini, F., and Pantosti, D. (2008). Twenty years of paleoseismology in Italy. *Earth-Science Reviews*, 88(1–2), 89–117.
657 <https://doi.org/10.1016/j.earscirev.2008.01.001>
- 658 Galli, P., Giaccio, B., Peronace, E., and Messina, P. (2015). Holocene paleoearthquakes and early-late pleistocene slip rate on the
659 Sulmona fault (Central Apennines, Italy). *Bulletin of the Seismological Society of America*, 105(1), 1–13.
660 <https://doi.org/10.1785/0120140029>
- 661 Galli, P., & Pallone, F. (2019). Reviewing the intensity distribution of the 1933 earthquake (Maiella, Central Italy). Clues on the seismogenic
662 fault. *Alpine and Mediterranean Quaternary*, 32(2), 93–100.
- 663 Ghisetti, F., and Vezzani, L. (1997). Interfering paths of deformation and development of arcs in the fold-and-thrust belt of the central
664 Apennines (Italy). *Tectonics*, 16(3), 523–536. <https://doi.org/10.1029/97TC00117>
- 665 Giaccio, B., Messina, P., Sposato, A., Voltaggio, M., Zanchetta, G., Galadini, F., Gori, S., and Santacroce, R. (2009). Tephra layers from
666 Holocene lake sediments of the Sulmona Basin, central Italy: implications for volcanic activity in Peninsular Italy and tephrostratigraphy
667 in the central Mediterranean area. *Quaternary Science Reviews*, 28(25–26), 2710–2733.
668 <https://doi.org/10.1016/j.quascirev.2009.06.009>
- 669 Giaccio, Biagio, Castorina, F., Nomade, S., Scardia, G., Voltaggio, M., and Sagnotti, L. (2013). Revised Chronology of the Sulmona
670 Lacustrine Succession, Central Italy. *Journal of Quaternary Science*, 28(6), 545–551. <https://doi.org/10.1002/jqs.2647>
- 671 Gori, S., Falcucci, E., Ladina, C., Marzorati, S., and Galadini, F. (2017). Active faulting, 3-D geological architecture and Plio-Quaternary
672 structural evolution of extensional basins in the central Apennine chain, Italy. *Solid Earth*, 8(2), 319–337.
- 673 Gori, S., Falcucci, E., Dramis, F., Galadini, F., Galli, P., Giaccio, B., Messina, P., Pizzi, A., Sposato, A., and Cosentino, D. (2014a). Deep-
674 seated gravitational slope deformation, large-scale rock failure, and active normal faulting along Mt. Morrone (Sulmona basin, Central
675 Italy): Geomorphological and paleoseismological analyses. *Geomorphology*, 208, 88–101.
676 <https://doi.org/10.1016/j.geomorph.2013.11.017>
- 677 Gori S. (2010). Definition of seismogenic sources in poorly known tectonically active regions of the Italian Peninsula". Ph.D. Thesis.
678 Università degli Studi Roma Tre. Tutor Prof. Francesco Dramis.
- 679 Gori, S., Giaccio, B., Galadini, F., Falcucci, E., Messina, P., Sposato, A., and Dramis, F. (2009). Active normal faulting along the Mt.
680 Morrone southwestern slopes (central Apennines, Italy). *International Journal of Earth Sciences*, 100(1), 157–171.
681 <https://doi.org/10.1007/s00531-009-0505-6>
- 682 Iezzi, F., Mildon, Z., Walker, J. F., Roberts, G., Goodall, H., Wilkinson, M., and Robertson, J. (2018). Coseismic Throw Variation Across
683 Along-Strike Bends on Active Normal Faults: Implications for Displacement Versus Length Scaling of Earthquake Ruptures. *Journal
684 of Geophysical Research: Solid Earth*, 123(11), 9817–9841. <https://doi.org/10.1029/2018JB016732>



- 685 lezzi, F., Francescone, M., Pizzi, A., Blumetti, A., Boncio, P., Di Manna, P., Pace, B., Piacentini, T., Papasodaro, F., Morelli, F., Caciagli,
686 M., Chiappini, M., D'Ajello Caracciolo, F., Materni, V., Nicolosi, I., Sapia, V. and Urbini, S. (2023) - Slip localization on multiple fault
687 splays accommodating distributed deformation across normal fault
688 complexities, *TECTONOPHYSICS*, 868, <https://doi.org/10.1016/j.tecto.2023.230075>
- 689 Lavecchia, G., Brozzetti, F., Barchi, M., Menichetti, M., and Keller, J. V. A. (1994). Seismotectonic zoning in east-central Italy deduced
690 from an analysis of the Neogene to present deformations and related stress fields. *Geological Society of America Bulletin*, 106(9),
691 1107–1120. [https://doi.org/10.1130/0016-7606\(1994\)106<1107:SZIECI>2.3.CO;2](https://doi.org/10.1130/0016-7606(1994)106<1107:SZIECI>2.3.CO;2)
- 692 Manighetti, I., Campillo, M., Bouley, S., & Cotton, F. (2007). Earthquake scaling, fault segmentation, and structural maturity. *Earth and
693 Planetary Science Letters*, 253(3-4), 429-438.
- 694 Martin, C. W., and Johnson, W. C. (1995). Variation in radiocarbon ages of soil organic matter fractions from late quaternary buried soils.
695 In *Quaternary Research* (Vol. 43, Issue 2, pp. 232–237). <https://doi.org/10.1006/qres.1995.1023>
- 696 Mattiocco E. (1981). Centri fortificati preromani nella conca di Sulmona. Ministero per i Beni Culturali e Ambientali. Soprintendenza
697 archeologica dell'Abruzzo.
- 698 McCalpin, J. P. (2009). Paleoseismology in extensional tectonic environments. *International geophysics*, 95, 171-269.
- 699 Miccadei, E., Barberi, R., and Cavinato, G. P. (1998). La geologia quaternaria della Conca di Sulmona (Abruzzo, Italia centrale). In
700 *Geologica Romana* (Vol. 34, pp. 59–86). [papers3://publication/uuid/6DCED5BC-C919-4D11-A92C-AAB0F98B9CF9](https://doi.org/10.1016/j.geologica.1998.09.001)
- 701 Miccadei, E., Paron, P., and Piacentini, T. (2004). The SW escarpment of Montagna del Morrone (Abruzzi, Central Italy): Geomorphology
702 of a fault-generated mountain front. *Geografia Fisica e Dinamica Quaternaria*, 27(1), 55–87.
- 703 Patacca, E., Sartori, R., and Scandone, P. (1990). Tyrrhenian basin and Apenninic arcs : Kinematic relations since Late Tortonian times.
704 *Memorie Della Societa Geologica Italiana*, 45, 425–451.
- 705 Piccardi, L., Gaudemer, Y., Tapponnier, P., and Boccaletti, M. (1999). Active oblique extension in the central Apennines (Italy): Evidence
706 from the Fucino region. *Geophysical Journal International*, 139(2), 499–530. <https://doi.org/10.1046/j.1365-246X.1999.00955.x>
- 707 Pizzi, A. and Pugliese, G. (2004) - InSAR-DEM analyses integrated with geologic field methods for the study of long-term seismogenic
708 fault behavior: Applications in the axial zone of the central Apennines (Italy). *JOURNAL OF SEISMOLOGY*, 8(3), pp. 313-329. DOI:
709 10.1023/B:JOSE.0000038454.18706.25
- 710 Pizzi, A., Falcucci, E., Gori, S., Galadini, F., Messina, P., Di Vincenzo, M., and Sposato, A. (2010). Active faulting in the Maiella massif
711 (central Apennines, Italy). *GeoActa*, 3, 57-73.
- 712 Pondrelli, S., Salimbeni, S., Morelli, A., Ekström, G., Olivieri, M., and Boschi, E. (2010). Seismic moment tensors of the April 2009, L'Aquila
713 (Central Italy), earthquake sequence. *Geophysical Journal International*, 180(1), 238-242.
- 714 Pucci, S., Villani, F., Civico, R., Di Naccio, D., Porreca, M., Benedetti, L., Gueli, A., Stella, G., Baccheschi, P., and Pantosti, D. (2019).
715 Complexity of the 2009 L'Aquila earthquake causative fault system (Abruzzi Apennines, Italy) and effects on the Middle Aterno
716 Quaternary basin arrangement. *Quaternary Science Reviews*, 213, 30–66. <https://doi.org/10.1016/j.quascirev.2019.04.014>
- 717 Pucci, S., Villani, F., Civico, R., Pantosti, D., Del Carlo, P., Smedile, A., De Martini, P. M., Pons-Branchu, E., and Gueli, A. (2015).
718 Quaternary geology of the Middle Aterno Valley, 2009 L'Aquila earthquake area (Abruzzi Apennines, Italy). *Journal of Maps*, 11(5),
719 689–697. <https://doi.org/10.1080/17445647.2014.927128>
- 720 Puliti, I., Benedetti, L., Pizzi, A., Fleury, J., Francescone, M., Guillou, V., and Team, A. (2024). Evidence for a constant slip rate over the
721 last ~ 40 ka along the Mt. Morrone Fault System in Central Apennines. 1–28. <https://doi.org/10.1029/2023TC007871>
- 722 Puliti, Irene, Pizzi, A., Benedetti, L., Di Domenica, A., and Fleury, J. (2020). Comparing Slip Distribution of an Active Fault System at
723 Various Timescales: Insights for the Evolution of the Mt. Vettore-Mt. Bove Fault System in Central Apennines. *Tectonics*, 39(9), 1–22.
724 <https://doi.org/10.1029/2020TC006200>
- 725 Puliti, Irene, Pucci, S., Villani, F., Porreca, M., Benedetti, L., Robustelli, G., Gueli, A., and Stella, G. (2022). Estimating the long-term slip
726 rate of active normal faults: The case of the Paganica Fault (Central Apennines, Italy). *Geomorphology*, 415, 108411.
727 <https://doi.org/10.1016/j.geomorph.2022.108411>
- 728 Ramsey, C. B. (2009). Bayesian analysis of radiocarbon dates. *Radiocarbon*, 51(1), 337–360.
729 https://doi.org/10.2458/azu_uapress_9780816530595-ch039
- 730 Regattieri, E., Giaccio, B., Nomade, S., Francke, A., Vogel, H., Drysdale, R. N., Perchiazzi, N., Wagner, B., Gemelli, M., Mazzini, I.,
731 Boschi, C., Galli, P., and Peronace, E. (2017). A Last Interglacial record of environmental changes from the Sulmona Basin (central
732 Italy). *Palaeogeography, Palaeoclimatology, Palaeoecology*, 472, 51–66. <https://doi.org/10.1016/j.palaeo.2017.02.013>
- 733 Reimer, P. J., Bard, E., Bayliss, A., Beck, J. W., Blackwell, P. G., Ramsey, C. B., Brown, D. M., Buck, C. E., Edwards, R. L., Friedrich, M.,
734 Grootes, P. M., Guilderson, T. P., Haffidason, H., Hajdas, I., Hatté, C., Heaton, T. J., Hogg, A. G., Hughen, K. A., Kaiser, K. F., ... van



- 735 der Plicht, J. (2013). Selection and Treatment of Data for Radiocarbon Calibration: An Update to the International Calibration (IntCal)
736 Criteria. *Radiocarbon*, 55(4), 1923–1945. https://doi.org/10.2458/azu_js_rc.55.16955
- 737 Reitman, N. G., Bennett, S. E. K., Gold, R. D., Briggs, R. W., and DuRoss, C. B. (2015). High-resolution trench photomosaics from image-
738 based modeling: Workflow and error analysis. *Bulletin of the Seismological Society of America*, 105(5), 2354–2366.
739 <https://doi.org/10.1785/0120150041>
- 740 Rovida, A., Antonucci, A., and Locati, M. (2022). The European preinstrumental earthquake catalogue EPICA, the 1000–1899 catalogue
741 for the European Seismic Hazard Model 2020. *Earth System Science Data Discussions*, 2022, 1–30.
- 742 Servizio Geologico d'Italia (2006). Carta Geologica d'Italia alla scala 1:50,000, F. 369 Sulmona. ISPRA, Roma.
743 https://www.isprambiente.gov.it/Media/carg/369_SULMONA/Foglio.html
- 744 Silvestri A. (2016). Il villaggio dell'età del Bronzo di Trasacco (AQ), nuovi dati. In: "Il Fucino e le aree limitrofe nell'antichità. Archeologia e
745 rinascita culturale dopo il sisma del 1915", Proceedings of the 4th Archaeological Workshop, Avezzano (Italy), 22-23 May 2015,
746 Archeoclub d'Italia, DVG Studio, Avezzano (Italy), pp. 171-184.
- 747 Van Wonerghem F. (1984). *Superaequum, Corfinium, Sulmo. Forma Italiae*, Unione Accademica Nazionale, Istituto di Topografia Antica
748 dell'Università di Roma. Editor L. Olschki.
- 749 Vignaroli, G., Rossetti, F., Petracchini, L., Argante, V., Bernasconi, S. M., Brilli, M., ... & Soligo, M. (2022). Middle Pleistocene fluid
750 infiltration with 10–15 ka recurrence within the seismic cycle of the active Monte Morrone Fault System (central Apennines, Italy).
751 *Tectonophysics*, 827, 229269.
- 752 Vittori, G.P. Cavinato, E. M. (1995). Active Faulting Along the Northerneastern edge of the Sulmona Basin, Central Appennines, Italy. In
753 *Perspectives in Paleoseismology* (pp. 115–125).
- 754 Wallace, R.E., 1987. Grouping and migration of surface faulting and varia- tions in slip rates on faults in the Great Basin Province. *Bulletin*
755 *of the Seismological Society of America* 77, 868±876
- 756 Wells, D. L., and Coppersmith, K. J. (1994). New empirical relationships among magnitude, rupture length, rupture width, rupture area,
757 and surface displacement. *Bulletin of the seismological Society of America*, 84(4), 974-1002.
- 758 Zavala, C. (2020). Hyperpycnal (over density) flows and deposits. *Journal of Palaeogeography*, 9(1). [https://doi.org/10.1186/s42501-020-](https://doi.org/10.1186/s42501-020-00065-x)
759 00065-x